Kansas State University

GODDARD GRANT
IN-43-CR
102766
64 P.

Annual Report

Estimating Regional Evapotranspiration from Remotely Sensed Data by Surface Energy Balance Models

Grant NAG 5-389

Principal Investigators

Ghassem Asrar

Edward Kanemasu

Duration

15 May 1986 to 14 Feburary 1987

Co-Investigators:

Dr. R. B. Myneni

Dr. R. L. Lapitan

Mr. T. R. Harris

Ms. J. M. Killeen

Mr. D. I. Cooper

Mr. C. Hwang

1. Report No.	2. Government Accession No.	3. Recipient's Catalog No.

4. Title and Subtitle	5. Report Date
Measurements of Micrometeorological Parameters for Testing Large-Scale Models: Estimating Regional Evapotranspiration from Remotely Sensed Data by Surface Energy Balance Models	6. Performing Organization Code
7. Author(s) Asrar et al.	8. Performing Organization Report No.
9. Performing Organization Name and Address Evapotranspiration Laboratory Kansas State University Manhattan, KS 66506	10. Work Unit No. 11. Contract or Grant No. NAG 5-389
12. Sponsoring Agency Name and Address NASA/Goddard Space Flight Center Code 624	13. Type of Report and Period Covered ANNUAL REPORT for 1986 14. Sponsoring Agency Code NASA/GSFC Code 624

15. Supplementary Notes

Technical Monitor
Dr. Robert Gurney

16. Abstract

Please refer to abstract on the following page.

17. Key Words (Suggested by Author(s))	18. Distribution Statement
Energy balance, reflectance, surface temperature, grassland	

19. Security Classif. (of this report)	20. Security Classif. (of this page)	21. No. of Pages	22. Price*
Unclassified	Unclassified	64	

*For sale by the National Technical Information Service, Springfield, Virginia 22161

Abstract

This report contains the results of research activities conducted under Grant NAG 5-389 during 15 May 1986 to 14 February 1987. The first chapter deals with spatial and temporal variations of surface radiative temperatures of the burned and unburned areas of the Konza tallgrass prairie. The role of management practices, topographic conditions and the uncertainties associated with in situ or airborne surface temperature measurements are assessed in this chapter. The second chapter deals with evaluation of diurnal and seasonal spectral characteristics of the burned and unburned areas of the prairie. This is accomplished based on the analysis of measured spectral reflectance of the grass canopies under field conditions, and modelling their spectral behavior using a one dimensional radiative transfer model.

CHAPTER ONE

Radiative Surface Temperatures of the Burned and Unburned Areas in a Tallgrass Prairie[+]

[+] This chapter has been accepted for publication in Remote Sensing of Environment.

Abstract

This study was conducted in a natural tallgrass prairie area in the Flint Hills of Kansas. Our objective was to evaluate the surface radiative temperatures of burned and unburned treatments of the grassland as a means of delineating the areas covered by each treatment. Burning is used to remove the senescent vegetation resulting from the previous year's growth. Surface temperatures were obtained in situ and by an airborne scanner. These data showed that the unburned grass canopy was typically warmer than the burned one. Measurements of surface energy balance components revealed a difference in partitioning of the available energy between the two treatments, which resulted in the difference in their measured surface temperatures. The magnitude of this difference is dependent on the time of measurements and topographic conditions.

Introduction

This study was conducted in preparation for the International Satellite Land Surface Climatology Project (ISLSCP), First Field Experiment (FIFE), which is scheduled for May - November, 1987. The overall objective of FIFE is to further evaluate in detail the use of remotely sensed data in estimating surface and near surface conditions/properties, based on the measured reflected and emitted radiation, for input to the biospheric components of regional and global atmospheric circulation models (Schmugge and Seller, 1986). Earlier studies (Carlson, 1981; Price, 1983) have evaluated the potential applications of satellite derived surface temperatures in estimation of surface energy balance, moisture availability, and thermal inertia from surface energy balance models.

In comparing the accuracy and resolution of remotely sensed signals obtained by airborne sensors with the corresponding ground-measured quantities, a complication may arise from their spatial and temporal differences. For example, the images that are obtained from airborne or space-based systems include primarily the spatial variation in surface/ near surface fluxes of reflected or emitted energy, for an instantaneous field of view. Characterization of the same areas by comparable ground measurements would include both spatial and temporal trends. These differences must be resolved for a meaningful interpretation of the remotely sensed signals and their effective application for assessing surfaces and near-surface conditions/properties.

The objective of this study was to assess the effects of removal (absence) of a layer of senescent vegetation, resulting from growth in the previous year(s), on spatial and temporal trends in surface radiative

temperatures in a tallgrass prairie. This is one of several requirements toward our ultimate objective of developing appropriate methods or models that account for the significant sources of variation associated with in situ measurements to obtain representative aerial averages for comparison with the remotely sensed airborne measurements.

Materials and Methods

Site Description:

The study site was the Konza Prairie Research Natural Area (KPRNA) located near Manhattan, Kansas (39° 9'N, 96° 40'W). This area has been selected for conducting the ISLSCP-FIFE experiments during May - November 1987. The predominant soils in this area are silty clay loam with variable depth and soil-water-retention characteristics (Bidwell and McBee, 1973).

This tallgrass prairie is composed of 3487 hectares of unplowed grassland with big bluestem (Andropogon gerardii Vitman), little bluestem (Andropogon scoparius Michx.), and Indian grass (Sorghastrum nutans (L.) Nash) as dominant species. Thirty-six other species have been observed in a detailed vegetation composition study (The Tallgrass Laboratory, 1984). Since human settlement about 125 years ago, the major treatments on the KPRNA have been grazing by wildlife and natural or controlled burning of senescent vegetation on some parts of the prairie.

The area has a temperate, mid-continental climate with warm, moist summers and cool, dry winters. Annual mean precipitation is 750 mm, but it has a one percent chance of being less than 460 mm or greater than 1400 mm (Henderson, 1971).

Surface Temperature Measurements

Surface radiative temperatures of burned and unburned areas of the

prairie were measured by handheld infrared thermometers (Everest Interscience, Model 110*) and an airborne scanner (NS001) during summer of 1985. The handheld thermometer had a 2^{o} field of view (FOV) and a spectral wavelength band of 8-14 μm, and it was held at 45^{o} from nadir at the time of measurements. The scanner was on board a C-130 aircraft sponsored by the National Aeronautics and Space Administration, and it had a spectral wavelength band of 10.9-12.3 μm a 2.5 milliradian instantaneous field of view (100^{o} FOV), which resulted in a pixel size of about 10 m^{2} by looking straight down (nadir) from an altitude of 1500 m.

Two adjacent areas of the tallgrass prairie were selected for ground measurements and extraction of surface temperatures from the airborne images. One of the two areas had a layer of senescent vegetation 0.12 m thick on the soil surface (unburned), which resulted from one or more previous years' growth. Green leaf area index of the unburned area was about 1.0. On the adjacent area (burned), the senescent vegetation was removed by means of burning in early spring prior to the resumption of new vegetative growth. Green leaf area index of the burned area was about 1.4. The two areas were separated by an access road (fire guard). Vegetation on the burned area was more vigorous and less heterogeneous as compared with the unburned area; however, both canopies were about 0.80 m tall. In situ surface temperatures were obtained along established transects that covered the major sections of the burned and unburned areas. The surface temperature data extracted from the aerial images were from pixels located inward from the boundaries of the two areas.

---

* Tradenames and model number are given for the benefits of reader. No endorsement intended.

In situ surface temperature data were recorded by a portable data acquisition system (Polycorder Omnidata, Model 516A). The handheld infrared thermometer was routinely checked before and after each set of measurements by measuring the temperature of a reference blackbody target. Air temperatures were recorded by a handheld thermometer before, during and after each set of surface temperature measurements.

Components of surface energy balance were measured above the burned and unburned treatments. Net radiation was measured with Swissteco net pyrradiometers. Latent and sensible heat fluxes were measured based on the Bowen-ratio surface energy balance approach, using two high-precision resistance-thermometer psychrometers mounted immediately and 1.0 m above the grass canopies. Position of the two psychrometers were exchanged once every 6 minutes to cancel the effect of sensor differences in measured fluxes. Soil heat flux was measured with heat-flow transducers placed at 0.05 m below the soil surface. Soil temperatures were measured, above the soil heat-flow transducers, for computing the heat storage in this layer and estimating the surface heat flux. Signal from all sensors were recorded by Hewlett-Packard data acquisition system composed of an HP-71B microcomputer, an HP-3421A analog to digital converter, a HP-9114A disk-drive, and a HP-2225B printer.

Data Analysis

Digital counts and equivalent calibration temperature data acquired by the NS001 scanner on 17-19 June, 1985 were extracted from the computer compatible tapes obtained from the Goddard Space Flight Center. From the calibration data linear regression equations were established between the digital counts and the blackbody equivalent temperatures for each scan line. Eight sites was selected inside each of the two (burned vs. unburned) areas,

and digital-number values were extracted from five contiguous pixels(i.e., a total of 40 pixels per treatment area) from the image of the scene. The blackbody equivalent temperatures computed from the digital counts were then corrected for emissivity and atmospheric attenuation, using the NESS-80 atmospheric model (Weinreb and Hill, 1980).

The surface energy balance data were processed based on the Bowen-ratio approach (Fritschen, 1965). The procedure suggested by Ohmura (1982) was used for filtering the data especially in early morning and evening when gradients of sensible and latent heat are very small (i.e. near neutral conditions).

Results and Discussion

Error Analysis

To assess the uncertainties associated with both in situ and aerial measurements, we carried out an error analysis. This was deemed necessary for quantification of the temperature differences that could be observed between the burned and unburned areas. To compute the uncertainty associated with in situ measurements, we considered instrument accuracy and precision, surface emissivity, and spatial and temporal variabilities of surface temperatures.

The accuracy and precision of the handheld infrared radiometer provided by the manufacturer were $\pm$ 0.5 ^{o}C and $\pm$ 0.1 ^{o}C, respectively. An estimate of combined spatial and temporal variabilities was computed from the available in situ measurements obtained during 17-19 June 1985. A surface temperature variance of 1.5$^{o}C^{2}$ was found for a 10 m^{2} area, comparable to the pixel size of the aerial scanner. The square root of this variance ($\pm$1.2^{o}C) gives a rough measure of uncertainty for combined spatial and short-term

temporal variances associated with the in situ measurements. We assumed the emissivity of green vegetation to be 0.98 $\pm$ 0.01. Typical green plant emissivities range from 0.97 to 0.99 (Oke, 1980). The temperature uncertainty associated with $\pm$ 0.01 unit of green vegetation emissivity is $\pm 0.7^{o}C$ (Phinney and Arp, 1979). The combined root-sum-square (RSS) uncertainty associated with in situ measurements by considering all of the above factors was found to be $\pm 1.5^{o}C$.

Similarly, the uncertainty associated with the factors that affect airborne scanner measurements were computed, based on the procedure stablished by Cooper et al. (1985). The instrument precision for the NS001 scanner was estimated to be $\pm 0.2^{o}C$, based on the noise equivalent change in temperature. Its calibration uncertainty was estimated to be $\pm 0.5^{o}C$. Intra-pixel variability was accounted for by taking the average of temperature differences between a central pixel and its eight adjacent neighboring pixels. The range of these average values was $\pm 0.5^{o}C$ to $\pm 1.0^{o}C$. We used the conservative value of $\pm 1.0^{o}C$ in our computations. Since the airborne scanner was in nadir position, it could view both the vegetation and the background (i.e., soil or senescent vegetation). This could result in larger variance in the recorded signals. To account for this, we assumed a $\pm$ 0.02 unit change in surface emissivity for the airborne data. The uncertainty associated with this emissivity change, based on the earlier values, would be $\pm 1.4^{o}C$. However, if the atmospheric attenuation were included in the uncertainty associated with the emissivity, it would be reduced to $\pm 1.0^{o}C$. This is due to a longer pathlength between the sensor and the surface, as compared with in situ measurements. The longer pathlength includes increased water vapor content in the atmosphere and, subsequently, further attenuation of the upwelling thermal energy. This results in a reduced effective emissivity of the surface (Price, 1984). The

RSS uncertainty associated with the airborne measurements was estimated to be $\pm 1.59^{o}C$, by taking account of all of the parameters discussed. The data used in the error analysis are summarized in Table 1. The aggregate RSS uncertainty associated with both in situ and aerial measurements is $\pm 2.18^{o}C$, assuming that these uncertainties are additive. This aggregate uncertainty should be used in expressing the aerial scanner temperature data in terms of in situ measurements or vice versa.

The computed RSS value for the NS001 scanner is the theoretical limit of uncertainty based on available information about the sensor, and it requires some form of validation. The validation was performed using a statistical comparision of in situ and scanner data sets. Two coincident data sets from 17 and 19 June were used to calculate statistical confidence limits derived from a group-comparison t-test. This gives a measure of variability of the in situ data as compared with the scanner data. The calculated confidence limits for the in situ and scanner data ranged from $-1.2^{o}C$ to $+2.2^{o}C$, which were smaller than or equal in magnitude to the aggregate RSS uncertainty. Thus, the variability of the in situ measurements would not contribute additional uncertainties to the RSS estimate for the scanner. If the confidence limits were larger than the RSS value, then RSS estimate would have had to be upwardly revised to reflect the additional variability in the in situ measurements.

In Situ Surface Temperatures

In situ, measured, air and surface temperatures for 19 June 1985 are presented in Figure 1. During the early hours of the day, surface temperatures of both burned and unburned grass canopies were warmer than that of the surrounding air. The grass canopy of the burned treatment was warmer than that of the unburned treatment during this period. At midday, both

canopies were at equilibrium with the surrounding environment; but, they were cooler than the air in the afternoon. The grass canopy of the burned treatment was cooler than that of the unburned canopy during this period. This trend was generally observed during the month of June, when soil water content was not limiting because of frequent rainfalls (150 mm rain during 14-29 June). The observed differences were not statistically significant, because of large variance associated with measured surface temperatures, especially for the unburned treatment.

Similar in situ data collected during the soil-water limiting periods in 1984 and 1985 showed that grass canopies were warmer than the surrounding environments from midmorning until midafternoon (Figures 2 and 3). The surface temperatures of the burned treatment were cooler than those of the unburned treatment during the morning hours, but the trend was reversed around midday. This is an opposite trend to the one observed during the periods with adequate soil water content (Figure 1). The standard deviations represented with vertical bars in Figures 1-3 depict the extent of spatial variability associated with each set of in situ measurements of surface temperature along the transects on relatively flat upland areas of the tallgrass prairie during a given period. These data suggest a greater spatial variation during wet than during dry periods (Figures 1-3).

Figures 4 and 5 show the components of surface energy balance measured over the burned and unburned treatments on 23 June 1985. Net radiation flux densities for both treatments were comparable (i.e. difference was less than 10 Wm^{-2}), partitioning of this available energy, however, was different between the two treatments. Sensible heat flux from the unburned area was about 45% greater than the burned area at midday; but, latent heat flux was about 18% smaller. Soil heat flux density was also 50% smaller for the unburned as compared with the burned treatment at midday. These differences

were primarily due to the layer of senescent vegetation which serves as a mulch-layer, over the soil surface in the unburned treatment. The net effect was increased surface radiative temperatures due to reduced evapotranspiration and increased sensible heat flux in the unburned treatment.

The standard deviations presented in figures 1-3, however, do not include the contributions of other variable features such as topography and soil types that exist in the prairie. These features are inherently present in data obtained by airborne platforms with large spatial resolutions. Figure 6 shows surface temperature differences between the burned and unburned treatments for four major topographical conditions that are present in the tallgrass prairie. These include uplands, relatively level land at the ridgetops; slopes; toe, a transition zone between slope and lowland; and lowland, relatively level land in valleys, but distant from stream beds. The typical length of the transects established on these four areas was 300-500 meters.

The surface temperatures for the unburned treatment were consistently greater than those of the burned treatment, regardless of topography. The magnitude of this difference was largest between two treatments for the lowland area, followed by toe, slope, and upland, respectively (Figure 6). The circled mean temperatures, however, are not statistically ($p=0.05$) significant. The significantly larger surface temperatures difference observed between the two treatments in the lowland and toe areas, as compared with the upland, can be attributed to less air movement in the valley bottom. The soils in the lowland area are typically deep and maintain a high level of water content, which results from horizontal and vertical seepage of water from the upland and slopes. Thus, lack of soil water as a cause of increased surface temperatures in the valley bottom area is ruled out; but, shallow soil depth and limited soil water could be the

cause of warmer surface temperatures on the slopes as compared with the upland area. The air movement on the surface of slopes is considerably greater than that in the lowland area.

Airborne Surface Temperatures

The surface temperatures obtained from the airborne scanner (NS001) measurements also demonstrate the difference between the burned and unburned treatments (Table 2). These data were obtained during the afternoon hours, at about 14:30 CST. The blackbody equivalent surface temperatures of the burned treatment were 3.2, 2.6, and 3.0°C cooler than those of the unburned treatment for 17, 18, and 19 June, respectively. These differences increased to 3.8, 3.2, and 3.8°C, respectively, after the blackbody equivalent temperatures were corrected for emissivity and atmospheric attenuation effects, using the NESS-80 atmospheric model (Weinreb and Hill, 1980). This is due, in part, to a longer atmospheric pathlength for the emitted thermal energy to reach the airborne scanner as compared with the handheld thermometer. The increased water vapor in the pathlength results in further attenuation of the upwelling thermal energy (Brower et al., 1976). These differences are greater than the RSS uncertainty (1.59°C) associated with the NS001 scanner. The in situ measured difference between the burned and unburned treatments was approximatly 2.5° C at 14:30 hours (Figure 1). This corresponds to a mean difference of 3.8° 2.19°C, based on the NS001 scanner data. These data suggest that it is possible to delineate the burned from unburned areas of the tallgrass prairie based on the measurements of their emitted thermal radiation by airborne or possibly space-based platforms. Burned areas of the grassland can be also distinguished from unburned areas by their spectral reflectance characteristics in the visible to middle infrared regions of the spectrum (Asrar et al., 1986).

The variance in surface temperatures of the burned treatment was consistently lower than that of the unburned treatment, based on both in situ and airborne measurements. This is attributed to the layer of senescent vegetation that was present on the soil surface in the unburned treatment. This mulch-like layer significantly affects the surface energy balance and soil water status of the grass canopy, and also results in a more diverse composition of grass versus nongrass species, as compared with the burned treatment (Hulbert, 1969; Knapp, 1984).

Summary and Conclusions

This study was conducted to assess the use of surface radiative temperatures of burned and unburned areas of a tallgrass prairie as a means of delineating the areas covered by each treatment. An analysis of the errors associated with the factors that affect both in situ and airborne measurements revealed that the uncertainties associated with the data obtained by both methods are of the same order of magnitude ($\pm$1.5-1.6^{o}C). This uncertainty is smaller than the existing mean surface temperature differences between the two treatments of the tallgrass prairie. The magnitude of in situ surface temperature differences between the two treatments was dependent on the time of measurements (daily and seasonal) and topographic conditions. In situ and airborne surface radiative temperatures, however, can be used to distinguish the burned from unburned areas of the tallgrass prairie. These results support our earlier findings that the areas covered by each treatment can be distinguished by their spectral characteristics in the visible to thermal infrared regions of the spectrum. The activities planned for ISLSCP-FIFE will provide more

comprehensive data sets for further evaluation of relating in situ point measurement to aerial averages.

Acknowledgement

We thank Mrs. Pat Chapman and Ms. Lori Ingmire for typing of the manuscript and Mrs. Janet Killeen for preparing the figures. Financial supports were provided by the National Aeronautics and Space Administration Grants NAG 5-389 and NGT 17-002-801.

References

Asrar, G., R.L. Weiser, D.E. Johnson, E. T. Kanemasu, and J.M. Killeen (1986), Distinguishing among tallgrass prairie cover types from measurements of multispectral reflectance, Remote Sens. Environ. 19: 159-169.

Bidwell, O. W., and C. W. McBee (1973), Soils of Kansas, Kansas Agric. Exp. Station, Dept. of Agron., Contribution No. 1359.

Brower, A.L., H.S. Gohrbrand, W. Pichel, T.L. Singnore and C. Walton (1976), NOAA Tests, Memorandum NESS 78 - Satellite derived sea-surface temperatures from NOAA Spacecraft. U. S. Dept. Commerce, NOAA, Washington, DC, 74 pp.

Carlson, T.N., J.K. Dodd, S.G. Benjamin, and J.N. Cooper (1981), Satellite estimation of the surface energy balance, moisture availability and thermal inertia, J. Appl. Meteorol. 20:67-87.

Cooper, D.I., J. M. Russo, E. M. Perry, T. N. Carlson and G.W. Peterson (1985), Measurement uncertainties associated with satellite-derived surface temperatures. Proceedings 17th Conf. on Agric. and Forrest Meteorol., Scottsdale, Arizona, 21-24 May, pp. 148-150.

Fritschen, L.J. (1965), Accuracy of evapotranspiration measurements by the Bowen ratio method. Bull. Int. Assoc. Sci. Hydol., 10:38-48.

Henderson, J.A. (1971), Annual precipitation probabilities in Kansas, Bulletin No. 14, Kansas Water Resources Board, Topeka, Kansas, 107 pp.

Hulbert, L.C. (1969), Fire and litter effects in undisturbed bluestem prairie in Kansas, Ecology 50:874-877.

Knapp, A.K. (1984), Postburn differences in solar radiation, leaf temperature and water stress influencing production in lowland tallgrass prairie, Am. J. Bot. 71:220-227.

Ohmura, A. (1982), Objective criteria for rejecting data for Bowen ratio flux calculations. J. Appl. Meteorol. 21:595-598.

Oke, T.R. (1980), Boundary Layer Climates, Methune and Company, New York, NY, 371 pp.

Phinney, and G.K. Arp (1979), Emissivity corrections for satellite-derived radiometric data. Lockheed Tech. Memo. No. LEC12394, Houston, Texas, 19 pp.

Price, J. C. (1983), Estimation of surface temperature from satellite thermal infrared data. Remote Sens. Environ. 13:353-361.

Price, J.C. (1984), Land surface temperature measurements from the split window channels of the NOAA-7 Advanced Very High Resolution Radiometer. J. Geophys. Res., 89:7231-7237.

Schmugge, T.J. and P.J. Sellers (Ed.) (1986), Experiment plan for the First ISLSCP Field Experiment: Report of FIFE Science Working Group. Hydrological Sciences Branch, Goddard Space Flight Center, Greenbelt, Maryland, 43 pp.

The Tallgrass Laboratory (1984), Konza Prairie, Division of Biology, Kansas State University, Manhattan, KS, 20 pp.

Weinreb, M. P. and M. L. Hill (1980), Calculation of atmospheric radiances and brightness temperatures in infrared window channels of satellite radiometers, NOAA Technical Report, NESS-80, U. S. Department of Commerce, Washington, D. C., 40 pp.

Table 1. Root sum square uncertainties (σ) for the handheld radiometer and airborne scanner.

Factor	Handheld Radiometer		Airborne Scanner	
	σ(°C)	σ^2(°C^2)	σ(°C)	σ^2(°C^2)
Instrument Precision	±0.1	0.01	±0.2	0.04
Calibration	±0.5	0.25	±0.5	0.25
Atmospheric Correction	N.A.	N.A.	±0.5	0.25
Spatial Variability	±1.2	1.44	N.A.	N.A.
Location Error	N.A.	N.A.	±1.0	1.00
Emissivity	±0.7	0.49	±1.0	1.00
Aggregate Uncertainty		2.19		2.54
Root Sum Square		± 1.50°C		±1.59°C

Table 2. Mean black-body equivalent and surface temperatures corrected for atmospheric attenuation effect and their associated standard deviation for the burned and unburned treatments of the tallgrass prairie. The data were obtained by the NS001 thermal scanner on board a C-130 airplane at an altitude of 1500 m in 1985.

Date	Treatment	No. of Observations	Surface Temp. (^{O}C) Black-body	Corrected
17 June	Burned	40	24.6±0.75	27.2±0.87
	Unburned	40	27.9±1.34	31.0±1.54
18 June	Burned	40	23.2±0.85	25.4±1.05
	Unburned	40	25.8±1.35	28.4±1.67
19 June	Burned	40	25.7±0.71	30.9±0.94
	Unburned	40	28.7±1.48	34.7±2.02

List of Figures

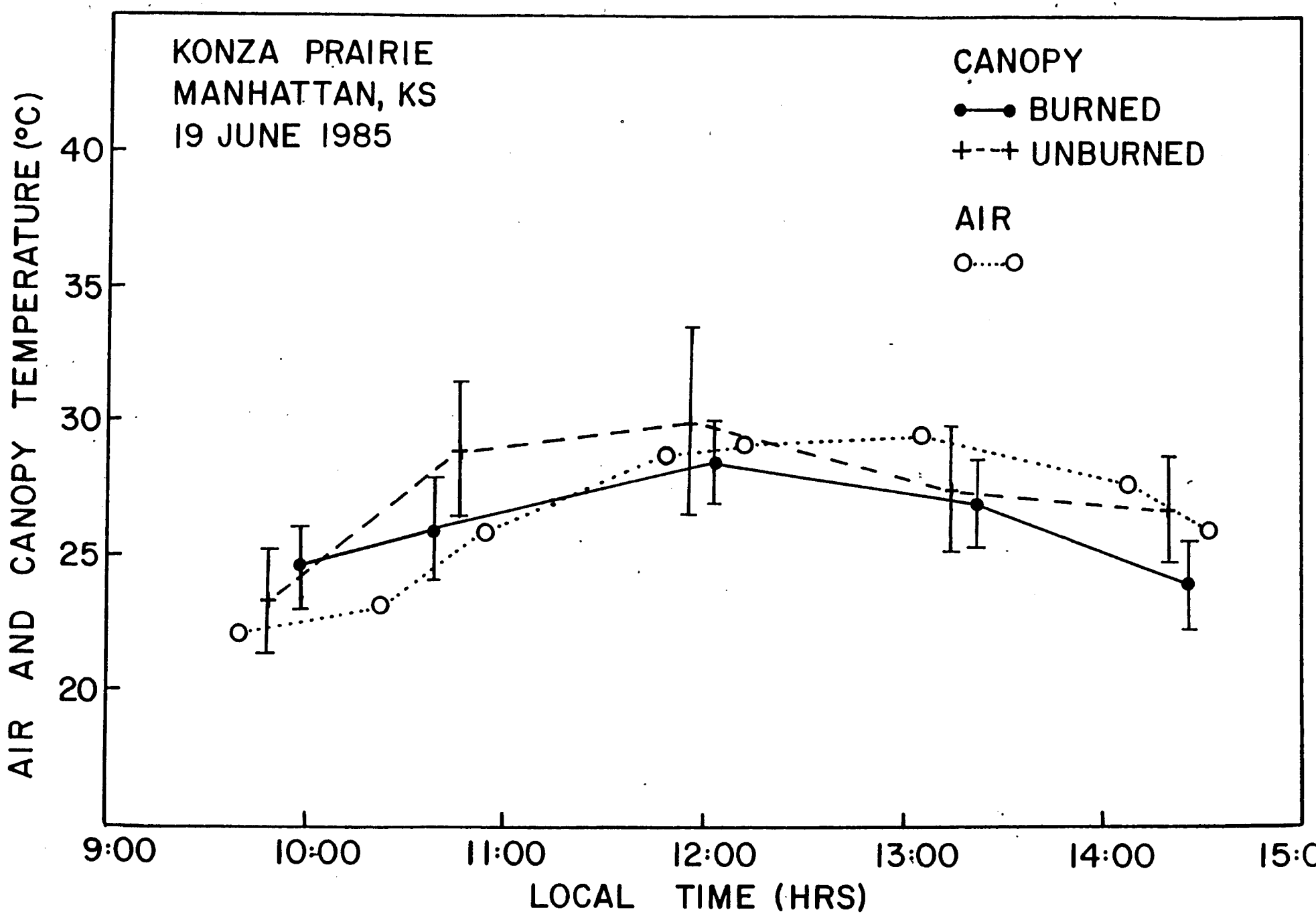
KONZA PRAIRIE
MANHATTAN, KS
19 JUNE 1985
CANOPY
BURNED
UNBURNED
AIR
AIR AND CANOPY TEMPERATURE (°C)
40
35
30
25
20
9:00
10:00
11:00
12:00
13:00
14:00
15:0
LOCAL TIME (HRS)

Fig. 1

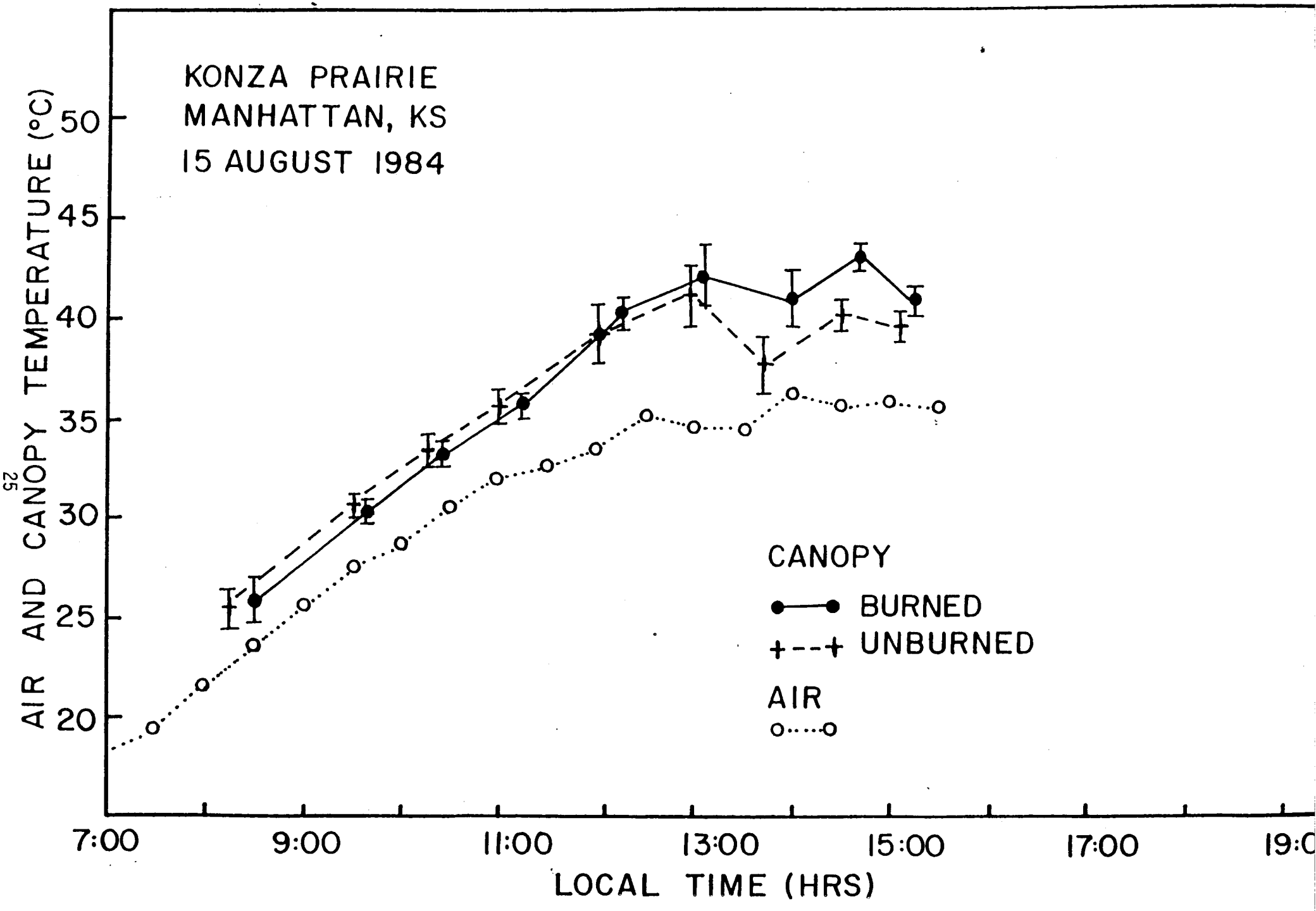
KONZA PRAIRIE
MANHATTAN, KS
15 AUGUST 1984
AIR AND CANOPY TEMPERATURE (°C)
50
45
40
35
30
25
20
CANOPY
BURNED
UNBURNED
AIR
7:00
9:00
11:00
13:00
15:00
17:00
19:0
LOCAL TIME (HRS)

Fig. 2

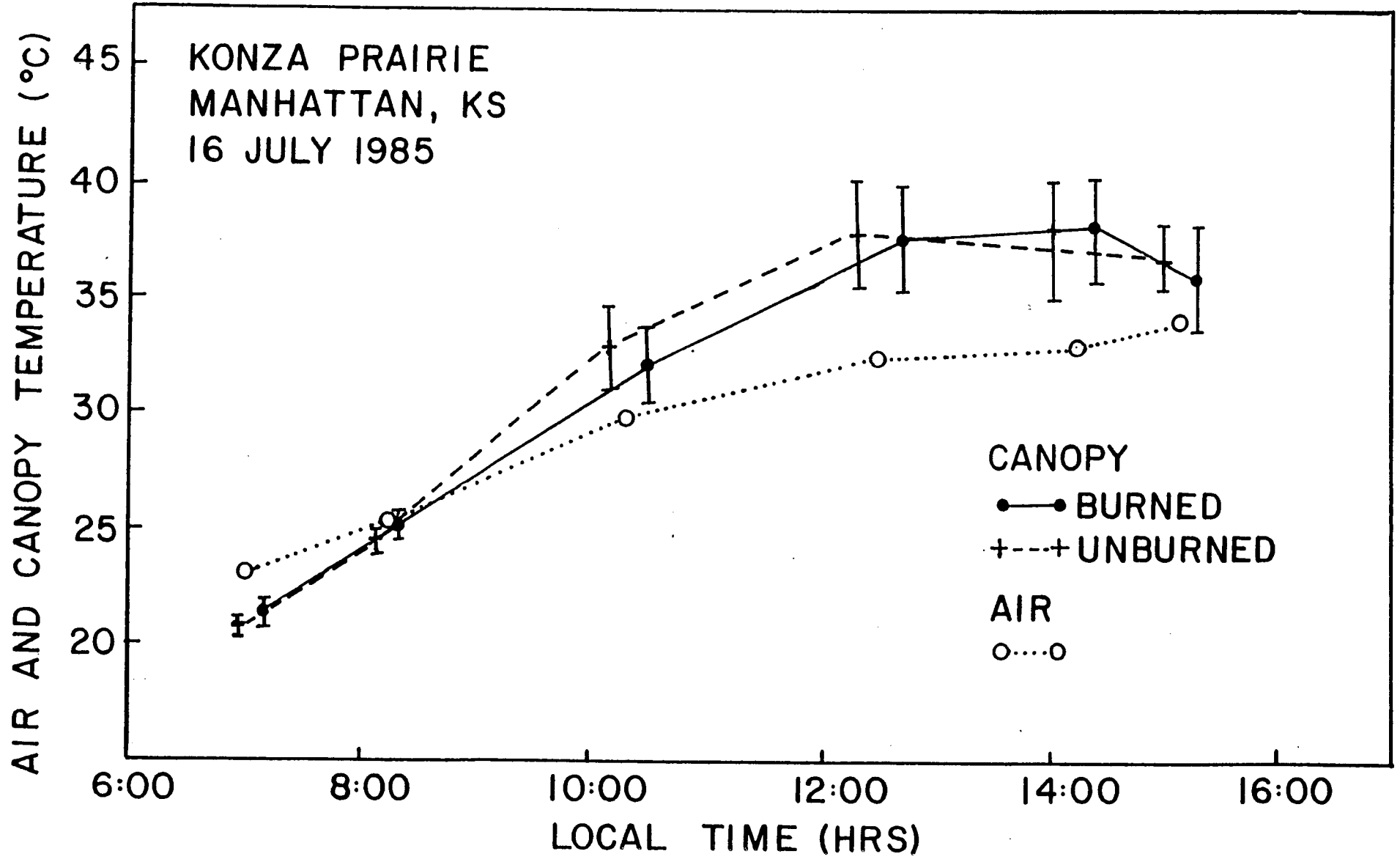
KONZA PRAIRIE
MANHATTAN, KS
16 JULY 1985
AIR AND CANOPY TEMPERATURE (°C)
45
40
35
30
25
20
6:00
8:00
10:00
12:00
14:00
16:00
LOCAL TIME (HRS)
CANOPY
BURNED
UNBURNED
AIR

Fig. 3

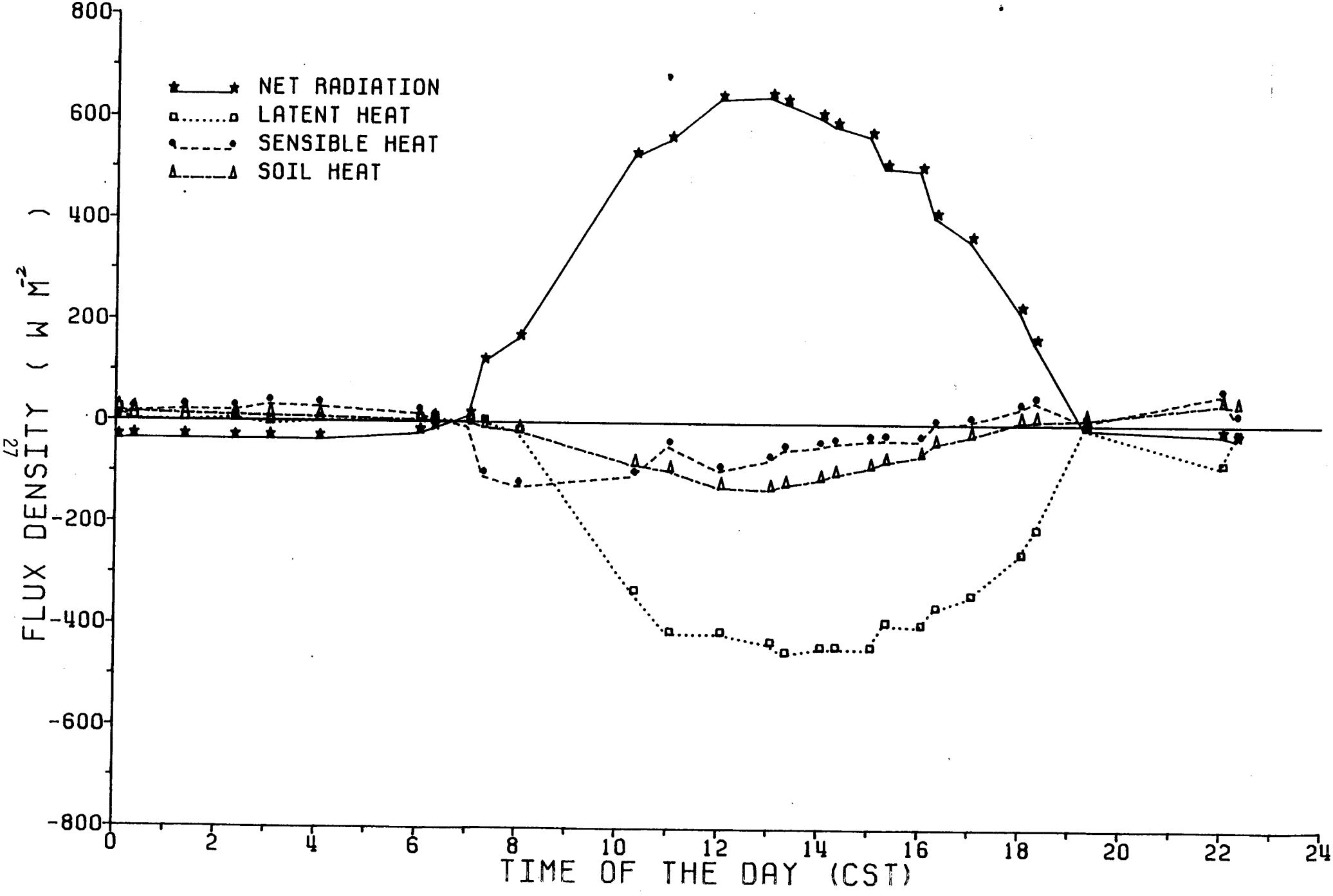
NET RADIATION
LATENT HEAT
SENSIBLE HEAT
SOIL HEAT
FLUX DENSITY (W M^{-2})
800
600
400
200
0
-200
-400
-600
-800
0
2
4
6
8
10
12
14
16
18
20
22
24
TIME OF THE DAY (CST)

Fig. 4

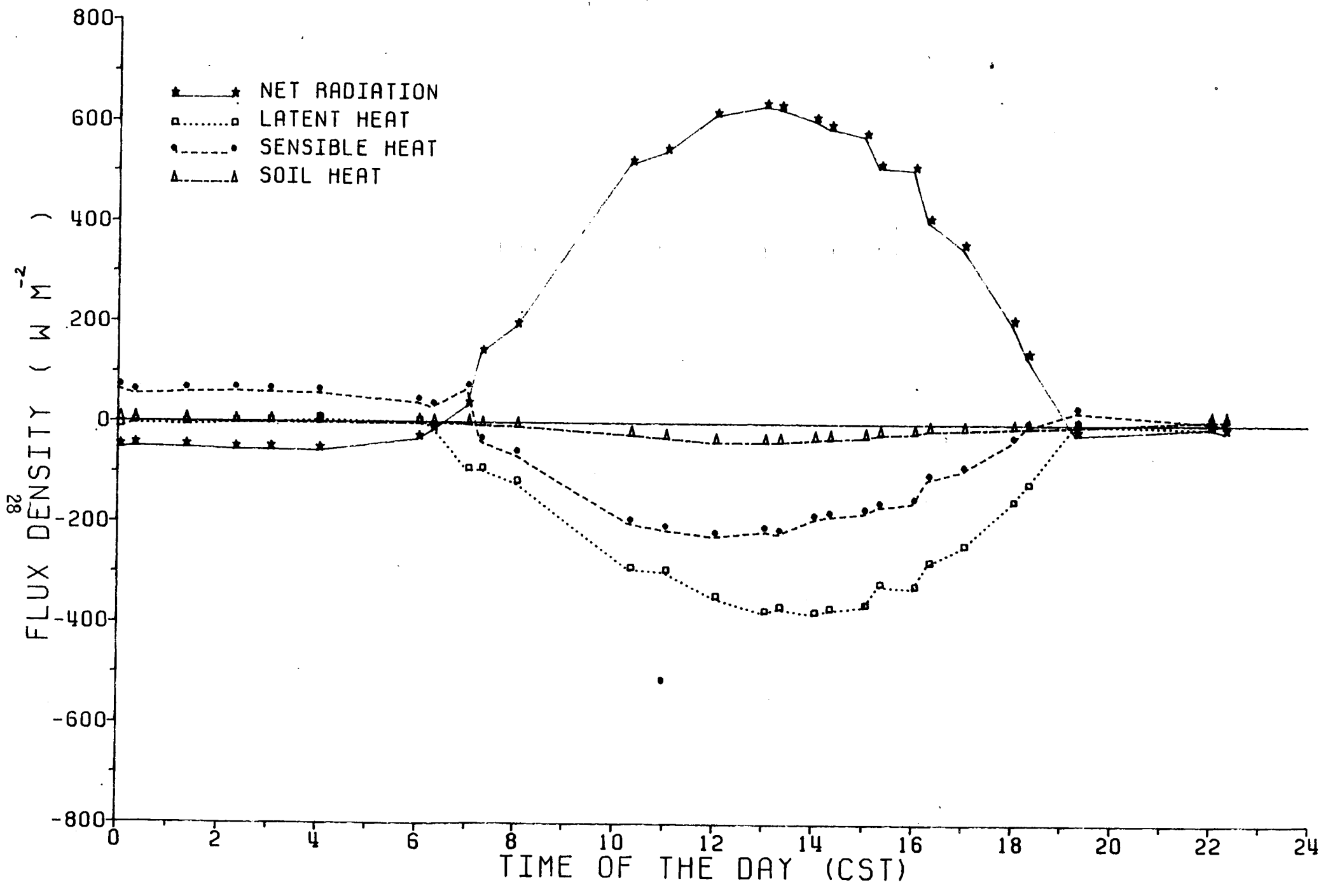
NET RADIATION
LATENT HEAT
SENSIBLE HEAT
SOIL HEAT
800
600
400
200
0
-200
-400
-600
-800
FLUX DENSITY (W M -2)
0
2
4
6
8
10
12
14
16
18
20
22
24
TIME OF THE DAY (CST)

Fig. 5

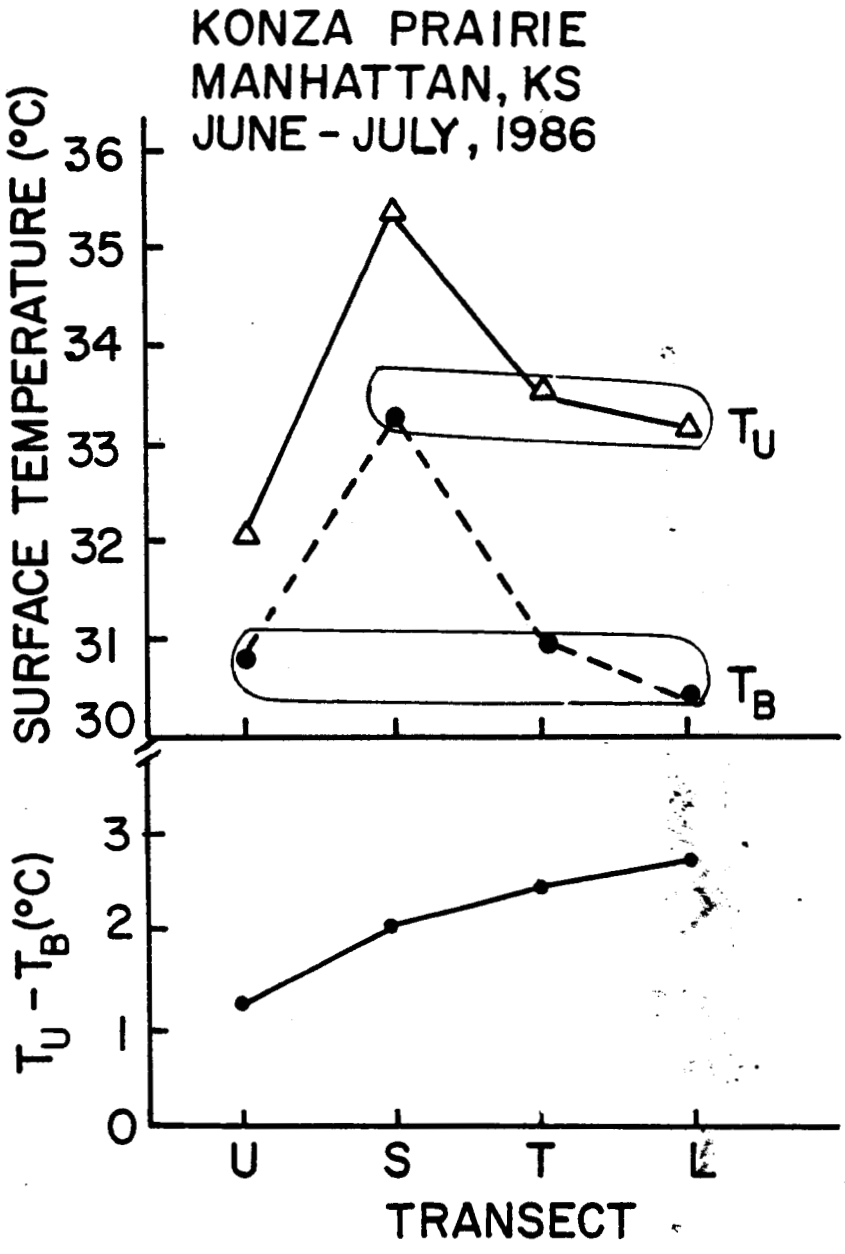
KONZA PRAIRIE
MANHATTAN, KS
JUNE - JULY, 1986
SURFACE TEMPERATURE (°C)
36
35
34
33
32
31
30
T_U
T_B
$T_U - T_B$(°C)
3
2
1
0
U
S
T
E
TRANSECT

Fig. 6

CHAPTER TWO

Measuring and Modelling Spectral Characteristics of a Tallgrass Prairie[+]

[+] This chapter has been accepted for publication in IEEE Transactions on Geoscience and Remote Sensing.

Abstract

This study was conducted to evaluate the diurnal and seasonal, spectral reflectance characteristics of burned and unburned areas of a tallgrass prairie, based on field measurements and models of radiation transport in the grass canopies. Burning of the senescent vegetation, resulting from the previous years' growth, is a common management practice, which results in improved productivity and affects the succession of grass species. The burned and unburned grass canopies showed distinctly different, diurnal and seasonal, spectral reflectance characteristics in the visible and infrared regions of the spectrum. These were attributed to the differences in development of the two plant canopies and the azimuthal differences in sensor-sun-canopy positions during field measurements of spectral reflectance. The radiation transfer model properly simulated the diurnal spectral behavior of the two canopies. The simulated, seasonal, spectral reflectance values for the unburned grass canopy were greater than the measured ones, because of limitations in proper representation of the layer of senescent vegetation in the model.

Introduction

Understanding the diurnal and seasonal patterns of spectral reflectance in a plant canopy plays a major role in the applications of remotely sensed data for inventory and management of natural resources. The non-Lambertian properties of plant canopies caused by their architecture affect the angular distribution of radiation reflected from them. This complicates the development and understanding of relationships between attributes of plant canopies and their spectral reflectance properties. Our present knowledge of how canopy reflectance may vary with different environmental and physiological factors derives from a combination of field measurements and modelling efforts.

A large number of studies have been conducted to investigate the effects of surface structure and environmental factors that contribute to the observed spectral reflectance characteristics of plant canopies. The effects of solar and view angles on plant canopy spectral reflectance have been studied for corn [1], cotton [2], soybean [3, 4], and wheat [5]. These studies showed that nadir and off-nadir reflectance measurements for complete or incomplete plant canopies vary greatly with the view-zenith and -azimuth angles. The diurnal effects on the measured canopy reflectance appeared to be less in the highly reflective (near infrared) wavelength bands than in the visible wavelengths. Thus, sun-view geometry has a more pronounced effect on the highly absorptive red (600-700 nm) wavelength band, especially for incomplete plant canopies. Similar results have been reported, based on the modelling of radiation transfer in plant canopies [6-11].

Pinter et al. [5] evaluated the effects of plant canopy architecture on diurnal and seasonal, spectral characteristics of several cultivars of spring wheat. They found that the visible to middle infrared reflectance from erectophile canopies was usually higher and varied more with changing sun azimuth and zenith angles than that from planophile canopies. The planophile wheat canopies had a more uniform spectral response throughout the day. The effects of solar angle and plant-canopy row orientation on spectrally estimated, green leaf area index of winter wheat canopies were evaluated by Asrar et al. [12].

The objective of this study was to evaluate the diurnal and seasonal spectral characteristics of burned and unburned treatments of a tallgrass prairie. This is a requirement for proper estimation of grass canopy attributes from spectral reflectance measurements.

Materials and Methods

Site Description:

Field studies were conducted in 1984 and 1985 in the Konza Prairie Research Natural Area (KPRNA) located in the Flint Hills of Kansas (39° 9'N, 96° 40'W). The predominant soil type in this area is silty clay loam (Udic Ustall), typical of the Flint Hills uplands [13]. KPRNA is 3487 ha of unplowed bluestem prairie, with big bluestem (Andropogon gerardii, Vitman), little bluestem (Andropogon scoparius, Michx.), and Indian grass (Sorghastrum nutans (L.), Nash) as the dominant species. Thirty-six other species of grasses, forbs, and small shrubs have been identified in detailed, vegetation composition studies [14].

The climate of the Flint Hills prairie is temperate, mid-continental, with warm, moist summers and cool, dry winters. Annual mean precipitation is 750 mm, but there is a one percent chance of it being less than 460 mm or greater than 1400 mm [15].

Two treatments were established in both years, on opposite sides of access roads (fireguards). On one side, the senescent vegetation from the previous year(s) was removed by burning in early spring (18-20 April), prior to the resumption of new growth. The area on the opposite side was left unburned, resulting in a layer of senescent vegetation that covered the soil surface. These two areas will be referred to as burned and unburned, respectively. The two treatments could be accessed only by north-south roads, with the burned and unburned treatments located on the west and east sides, respectively, in 1984. The position of the two treatments was reversed in 1985.

Data Acquisition:

Spectral reflectance and plant canopy parameters were collected in 1984 and 1985 at the locations described above. Spectral reflectance measurements were obtained with a Barnes[+] multimodular (model 15-1000) radiometer with 15° field of view at several viewing angles (nadir, 15°, 30° and 45°), using a truck-mounted platform. This radiometer has three discrete wavelength bands in the visible (450-520, 520-600 and 630-690 nm), two in the near infrared (760-900 and 1150-1300 nm), and two in the middle infrared (1550-1750 and 2080-2350 nm) regions of the

[+]Trade names are given for reference. No endorsement intended.

electromagnetic spectrum. The elevation of the radiometer at the time of measurements was 8 m above the soil surface. Canopy reflectance measurements were replicated 20 times on each treatment mostly during midday (11:00 a.m. to 14:00 p.m., CST), and referenced sequentially to a painted $BaSO_4$ calibration panel. The spectral measurements were made at least once a week (seasonal) and one to four times during selected days (diurnal), when sky conditions were clear. Spectral reflectance and transmittance of individual green leaves of grass and non-grass species were measured in the discrete wavelength bands that correspond to the Barnes radiometer, by a special spectroradiometer.

Nine plant samples, each including 0.1 m^2 of ground area, were obtained from nine locations on each of the two treatment transects. These sites were marked to avoid resampling and measuring of spectral reflectance in the future. In the laboratory, the plant samples were separated into green grass and non-grass and senescent vegetation. Total green leaf area of both grass and non-grass species was determined, using an optical area meter (LiCor, model LI-1300). A cubic spline procedure [16] was applied to smooth these measured values of green leaf area over time.

Theory

The transport of photons through a host medium, such as a plant canopy, can be represented by the linearized Boltzmann equation (hereafter called the transport equation). The analytic time-independent transport equation is simply a mathematical statement of particle conservation and expresses the change in the number of particles in a system as the difference between their production (by scattering) and

loss (by streaming or by capture) for a point in space at a particular energy level.

We consider a horizontally homogeneous, plane-parallel (stratification perpendicular to the Z-coordinate slab-geometry), optically anisotropic, vegetation canopy of finite physical thickness, filled densely and randomly with metameric leaf elements. The leaf orientation is assumed to be random, i.e., the normals to the upper face of the leaves are distributed uniformly along both polar coordinates. The slab is considered to be illuminated by collimated beams of monoenergetic photons (direct sunlight) and by a diffuse hemispherical source (the sky flux). Further, the slab is treated as being bounded by a reflecting soil or senescent vegetation boundary at the bottom (L_c: the leaf area index of the canopy). For this slab, we may write the following transport equation (a complete derivation is given in [11])

$$\frac{\mu}{G}\,\frac{dI(L;\underline{\Omega})}{dL} = I(L;\underline{\Omega}) - J(L;\underline{\Omega}) - Q(L;\underline{\Omega}), \qquad (1)$$

where

μ = cosine of solar zenith angle (θ); $\mu \in (-1,0)$ corresponds to descending directions and $\mu \in (0,1)$ corresponds to ascending directions;

$\underline{\Omega}$ = unit vector, denoting a direction located in polar coordinates by $[\mu,\phi]$, where ϕ is the zenith angle;

L = cumulative leaf area index; accumulated from top downwards;

I = specific intensity or angular flux.

The $G(\underline{\Omega})$ function determines the area projected on a plane perpendicular to the direction $\underline{\Omega}$ by a unit leaf area in the canopy [20]. In

the case of uniform leaf normal distribution we have

$$G(\underline{\Omega}) = G = \frac{1}{2\pi}\int_0^{2\pi} d\phi_L \int_0^1 d\mu_L \; | \underline{\Omega}_L \cdot \underline{\Omega} | = 0.5 \; . \qquad (2)$$

The distributed source term $J(L;\underline{\Omega})$ is

$$J(L;\underline{\Omega}) = \frac{\omega}{4\pi}\int_0^{2\pi} d\phi' \int_{-1}^1 d\mu' \; I(L;\underline{\Omega}') \; P(\underline{\Omega}' \rightarrow \underline{\Omega}) \, , \qquad (3)$$

where ω is the single scattering albedo by the leaves. The scattering phase function $P(\underline{\Omega}' \rightarrow \underline{\Omega})$ is

$$P(\underline{\Omega}' \rightarrow \underline{\Omega}) = 4 \int_0^{2\pi} d\phi_L \int_0^1 d\mu_L \; | \underline{\Omega}_L \cdot \underline{\Omega}' | \; | \underline{\Omega}_L \cdot \underline{\Omega} | \qquad (4)$$

and normalizes to

$$\frac{1}{4\pi}\int_0^{2\pi} d\phi \int_{-1}^1 d\mu \; P(\underline{\Omega}' \rightarrow \underline{\Omega}) \equiv 1.0, \qquad (5)$$

which states that for any incident direction, a scattered photon will have unit probability of being deflected into some outbound path.

The external first-collision source term $Q(L;\underline{\Omega})$ is the sum of four independent first-collision source terms,

$$Q(L;\underline{\Omega}) = \frac{\omega}{4\pi} \pi I_0 \; P(\underline{\Omega}_0 \rightarrow \underline{\Omega}) \exp \{ \; GL/\mu_0 \; \} \; +$$

$$+ \frac{\omega}{4\pi} \pi I_d \int_0^{2\pi} d\phi' \int_{-1}^0 d\mu' \; P(\underline{\Omega}' \rightarrow \underline{\Omega}) \exp \{ \; GL/\mu' \; \} \; +$$

$$+ \frac{\omega}{4\pi} \pi I_{r0} \int_0^{2\pi} d\phi' \int_0^1 d\mu' \; P(\underline{\Omega}' \rightarrow \underline{\Omega}) \exp \{ \; -G(L_c - L)/\mu' \; \} \; +$$

$$+ \frac{\omega}{4\pi} \pi I_{rd} \int_0^{2\pi} d\phi' \int_0^1 d\mu' \, P(\underline{\Omega}' \rightarrow \underline{\Omega}) \exp \{ -G(L_c - L)/\mu' \}, \qquad (6)$$

where $\underline{\Omega}_0$ is a unit vector denoting the direction of incident collimated flux. I_o is the intensity of direct sunlight propagating along $\underline{\Omega}_o$, and it is estimated as

$$I_0 = -(\beta F) / (\mu_0 \pi), \qquad (7)$$

where β is the fraction of direct sunlight in the total incident flux density F. I_d is the intensity of diffuse sky flux, assumed here to be isotropic and is estimated as

$$I_d = (1-\beta)F / \pi . \qquad (8)$$

I_r is the intensity of isotropically reradiated flux from the soil surface. I_{ro} is due to uncollided propagation of direct sunlight through gaps in the canopy to the soil surface,

$$I_{r0} = -(1/\pi) \, r_s \, \mu_0 \, \pi I_0 \, \exp \{ GL_c/\mu_0 \}, \qquad (9)$$

where r_s is the soil hemispherical reflectance. Similarly, I_{rd} is due to uncollided propagation of diffuse skylight to the soil surface,

$$I_{rd} = -(1/\pi) \, r_s \, 2\pi \, I_d \int_{-1}^{0} d\mu \, \mu \exp \{ GL_c/\mu \} . \qquad (10)$$

There is no analytical solution to the transport equation (Eq.1); hence, we resort to a numerical solution. The method of discrete

ordinates is a very powerful and general tool for the deterministic solution of the complicated and refractory transport equation. In this method, the angular dependence of the transport equation is approximated by discretizing the angular variables μ and ϕ into a set of NxM discrete directions $\{\mu_i;\phi_j\}$. The set of corresponding weights is denoted by $[w_i;w_j]$. The spatial variable L is discretized into a set of K spatial nodes. The spatial derivative of Eq. 1 is now approximated by a finite difference scheme. The cell-centered flux is computed from the cell-edged values, using the diamond difference relations. The finite difference form of the discrete ordinates transport equation is now

$$\frac{\mu_i}{G\,\Delta_{k+\frac{1}{2}}}\{ I(L_{k+1};\underline{\Omega}_{ij}) - I(L_k;\underline{\Omega}_{ij}) \} = 0.5\{ I(L_{k+1};\underline{\Omega}_{ij}) + I(L_k;\underline{\Omega}_{ij}) \} -$$

$$- J(L_{k+\frac{1}{2}};\underline{\Omega}_{ij}) - Q(L_{k+\frac{1}{2}};\underline{\Omega}_{ij}) \; ; \; k=1,\ldots,K; \; i=1,\ldots,N \text{ and } j=1,\ldots,M, \quad (11)$$

where $J(L_{k+1};\underline{\Omega}_{ij})$ and $Q(L_{k+1/2};\underline{\Omega}_{ij})$ are discrete analogs of the distributed and first-collision source terms. These source terms are evaluated by the exact kernel technique, which involves computation of a transfer matrix composed of scattering cross sections for every $\underline{\Omega}_{nm} \rightarrow \underline{\Omega}_{ij}$ transfer (for details see [11]). Equation 11 may be solved for $I(L_{k+1};\underline{\Omega}_{ij})$ in terms of $I(L_k;\underline{\Omega}_{ij})$ as

$$I(L_{k+1};\underline{\Omega}_{ij}) = A_i\, I(L_k;\underline{\Omega}_{ij}) - B_i\{ J(L_{k+\frac{1}{2}};\underline{\Omega}_{ij}) + Q(L_{k+\frac{1}{2}};\underline{\Omega}_{ij}) \} \; ; \; \mu < 0 \quad (12)$$

and for $I(L_k;\underline{\Omega}_{ij})$ in terms of $I(L_{k+1};\underline{\Omega}_{ij})$ as

$$I(L_k;\underline{\Omega}_{ij}) = (1/A_i)\, I(L_{k+1};\underline{\Omega}_{ij}) + C_i\{ J(L_{k+\frac{1}{2}};\underline{\Omega}_{ij}) + Q(L_{k+\frac{1}{2}};\underline{\Omega}_{ij}) \} \; ;$$

$$\mu > 0, \quad (13)$$

where

$$A_i = \{ 1 + f_i \} / \{ 1 - f_i \} \tag{14}$$

$$B_i = \{ 2f_i \} / \{ 1 - f_i \} \tag{15}$$

$$C_i = \{ 2f_i \} / \{ 1 + f_i \} \tag{16}$$

$$f_i = \frac{G \, \Delta_{k+\frac{1}{2}}}{2\mu_i} \quad . \tag{17}$$

It should be noted here that Eq.12 is used for forward sweep of photons into the canopy and Eq. 13 is used for backsweep out of the canopy. In order to ensure positivity of the computed flux, the negative flux-fixup procedure employed was to simply set the offending flux to zero. This method was found to be superior to weighting the diamond difference relations [11]. From a knowledge of the boundary conditions, Eq. 12 and 13 can be used to iteratively solve the transport equation. A convergence criterion of 10^{-6} was used for all the computation discussed in the following section. Programming details are discussed in detail in a previous report [11].

Results and Discussion

Model Validation:

The discrete ordinates exact kernel techniques for one- and two-angle photon transport were coded in FORTRAN-77 as ONEVEG and TWOVEG, respectively, with the phase function code embedded in them.

After testing for photon flux conservation, we did some standard problems in atmospheric photon transport to validate the results of our codes by comparison with the benchmark results tabulated by Van de Hulst [17]. The results of Van de Hulst are for homogeneous, finite atmospheres illuminated by a uniformly symmetric, conical source with vacuum boundary conditions. The spatial variable L in our case corresponds to the optical depth of Van de Hulst when G=1, and further, we impose vacuum boundary conditions simply by letting r_s=o. In this case, the incident flux density F is equal to unity, and there is no diffuse skyflux (β =1). It should be emphasized here that the results of this validation exercise are for the one-angle problem (i.e., the azimuthally average of the two-angle problem).

The phase function used by Van de Hulst [17] is the azimuthal average of the Henyey-Greenstein phase function,

$$P(\mu' \rightarrow \mu) = \frac{1}{2\pi} \int_0^{2\pi} d\phi \, \frac{(1-g^2)}{\{1+g^2-2g \mid \underline{\Omega}\cdot\underline{\Omega}' \mid\}^{3/2}} , \tag{18}$$

where g is the anisotropy parameter. We chose three values for g; 0 (isotropic scattering), 0.5, and 0.75 (strongly anisotropic forward-scattering). Van de Hulst [17] tabulated the solutions of the multiple scattering problem as reflection (R) and transmission (T) functions,

$$R(\mu,\mu_0) = -I(0;\mu) / \mu_0 I_0 \qquad ; \mu > 0 \tag{19}$$

$$T(\mu,\mu_0) = -I(L_c;\mu) / \mu_0 I_0 \qquad ; \mu < 0 , \tag{20}$$

where $I(o,\mu)$ is the reflected angular flux at the top and $I(L_c,\mu)$ is

diffusively transmitted angular flux at the bottom of the medium. The reflection and transmission functions for $\tau = 2, \omega = 1, \mu_o = -1.0$ and -0.1 are plotted in Figures 1 through 4. In all cases, the correspondence between the results of our discrete ordinates, exact kernel method and those tabulated by Van de Hulst is very good; the maximum relative difference was less than one-tenth of one percent.

The reflection functions shown in Figures 1 and 2 display physically sound characteristics. The reflected angular flux increases with increase in exit zenith angle, and this increase is steeper for oblique incident flux zenith angle. This effect arises because, as becomes smaller (oblique directions), the slab thickness increases and, hence, more scattering occurs into the reflected direction. However, as the slab encountered by the particles becomes thick enough that a significant number of collisions-absorptions occur, the particles disappear before reaching the top of the slab (an effect known as limb darkening [18]); see Figure 1 for $\mu \to o$. For more details on the validation of these codes, see our previous report [11].

The scattering phase function $[P(\underline{\Omega}' \to \underline{\Omega})]$ of a leaf layer in which the leaves are completely at random is plotted in Figure 5. An eight order quadrature (DP_8) set was used, and only the first 300 points are plotted. The phase function is notationally invariant as expected (the noise is numerical). The anisotropy in the scattered flux is evident, with relatively more scattered photons introduced in directions $(\pm\mu, \phi)$ close to the incidence direction $[\underline{\Omega} \cdot \underline{\Omega}' \to \pm 1]$. The phase function is symmetric about $\underline{\Omega} \cdot \underline{\Omega}' = o$, and, hence, the backscattered fraction is equal to the forward-scattered fraction, which is a consequence of the assumption $r_L = t_L = \omega/2$, where r_L and t_L are the leaf hemispherical reflectance

and transmittance.

Field Measurements:

The burned and unburned grass canopies showed distinctly different diurnal spectral characteristics in the visible and near to middle infrared regions of the spectrum (Figures 5 and 6). In the visible region (630-690 nm), the measured reflectance of the unburned treatment increased throughout the day for off-nadir viewing angles (i.e., 15^{o}, 30^{o} and 45^{o}). This trend was more distinct for the 30^{o} and 45^{o} than the 15^{o} viewing angles (Figure 6). The diurnal trend in spectral characteristic of the burned treatment was completely opposite. The reflectance from the burned canopy decreased consistently throughout the day (Figure 7), except for the nadir measurement which increased by 1% from early morning to midafternoon. The decreasing trend was more distinct for 30^{o} and 45^{o} than for 15^{o} viewing angles. The diurnal change in spectral reflectance of both treatments was least at nadir.

The opposite trend observed in spectral characteristics of the two canopies resulted from the position of the radiometer with respect to the sun and the canopies. The two treatments could be only accessed for measurement purposes by a north-south road, with the burned and unburned treatments located on the west and east sides of the road, respectively. During the morning hours, the radiometer was positioned in a hemisphere opposite to the sun for the burned treatment, recording mostly the forward scattered flux of the reflected radiation. The radiometer was in the same hemisphere as the sun for the unburned treatment, and it recorded predominantly the backscattered radiation during the morning hours. Thus, the azimuthal difference between the sensor-sun-canopy resulted in the different trends observed for the visible reflectance

characteristics of the two canopies. It should be noted that the difference between the canopies was more pronounced in early morning and mid-afternoon hours (Figs. 6 and 7), when contribution from the background was minimum, especially for off-nadir measurements. This suggests that there were some basic structural differences between the two canopies. Presence of the senescent vegetation on the soil surface in unburned treatment could also have contributed to these differences. This is particularly evident in comparing the nadir red reflectance (i.e., solid circles in Figs. 6 and 7) of the unburned canopy which was about 3% greater than the burned canopy during the morning hours. This difference diminished throughout the day, but the unburned treatment had consistently higher red reflectance for nadir view angle.

The near infrared diurnal spectral characteristics of the two treatments were also different (Figures 5 and 6). During the morning hours, the near infrared reflectance of the unburned treatment decreased, then it increased continuously from midmorning until midafternoon. The magnitude of reflectance values for a given viewing angle was comparable for the early morning and afternoon measurements. This is expected, because of symmetrical optical properties of the atmosphere around solar noon, during clear days. The near infrared reflectance from the burned treatment decreased from early morning until midday, then it stayed constant until midafternoon. The measured reflectances at nadir showed the smallest change throughout the day for both treatments. Diurnal spectral characteristics of the two treatments in the middle infrared (1550 - 1750 nm) were the same as in the near infrared region (Figures 5 and 6).

The difference in diurnal characteristics of the two treatments in the near to middle infrared regions can be attributed to the azimuthal

differences between the sensor-sun-canopy and the layer of senescent vegetation that covered the soil surface in the unburned treatment. This layer of senescent vegetation acts as a layer of sponge with large interstices, which extinguish the impinging solar radiation reaching the bottom of the grass canopy. The separation observed between the near and middle infrared reflectance of the unburned treatment is attributed to the opaque character of the senescent vegetation to the exiting radiation.

Measurement vs. Model Results:

The simulated, diurnal, canopy reflectances of the two treatments at an oblique viewing angle (47.9^{o}), for two selected days in 1984 and 1985, are presented in Figures 7 and 8, respectively. In the visible region, the unburned treatment had consistently higher reflectance than the burned treatment for each date, as well as for the two years. The difference observed between the burned and unburned treatments is attributed to the layer of senescent vegetation and the difference in distribution and magnitude of the green leaf area index of the two treatments, especially in 1985. The effect of senescent vegetation in the unburned canopy reflectance is particularly evident in 1984 data, since both canopies were at peak greenness. The strong absorption of radiation by plant pigments resulted in smaller red reflectance from the burned treatment, which had substantially greater green phytomass in both years.

Figure 8 shows the simulated near infrared reflectance from the two grass canopies for 1984 and 1985. In both years, the near infrared reflectance from the burned treatment decreased during the morning hours, then it plateaued at midday. The reflectance from the unburned

treatment showed a consistent decrease throughout the day in both years. The unburned treatment had a higher near infrared reflectance than the burned treatment in 1984; however, this trend was reversed in 1985. This was due to a larger green leaf area (LAI=1.47) for the burned than for the unburned (LAI=0.97) treatment. In this case, higher reflectance from the background senescent vegetation was offset by the reduced green leaf area of the unburned treatment in 1985. If the green leaf area of the two treatments had been comparable, as in 1984, the near infrared reflectance from the unburned treatment would have been consistently greater than that from the burned treatment. It should be noted that in our modelling effort, we did not include the layered structure of the senescent vegetation; it was considered merely as a flat surface with uniform spectral characteristics in this region of the spectrum.

The seasonal trends in spectral characteristics of the burned and unburned treatments in the visible and near infrared regions of the spectrum are presented in Figures 9 and 10. The connected data points are the simulated results from the radiative transfer model and the points with standard deviation bars are the measured data at ± 1 hour around solar noon. In general, the red reflectance decreased and near infrared reflectance increased with increased green leaf area index of the treatments, in both years. This was expected, since development of a grass canopy is accompanied by strong absorption of the visible and increased reflectance of near infrared radiation. The unburned treatment had consistently greater red reflectance than the burned treatment, at comparable LAI, both based on the measured and simulated results. This was due to the background senescent vegetation, which typically has a greater red reflectance than the bare soil [19].

The simulated, near infrared reflectance values for the unburnedtreatment were greater than those of the burned treatment in both years;however, the measured values for the unburned treatment were smaller than those of the burned treatment (Figure 10). This disagreement between the measured and simulated infrared reflectance data is partly due to the method of representation of background senescent vegetation in the radiation transfer model. We assumed that the layer of senescent vegetation is uniformly flat and Lambertian. This is a simplified representation, since this layer is like a sponge with very large interstices, which further extinguish the flux that reaches to the bottom of grass canopy. A more realistic representation of this layer is currently being explored.

Summary and Conclusions

The objective of this study was to evaluate the diurnal and seasonal, spectral characteristics of burned and unburned areas of a tallgrass prairie by direct field measurements and modelling. A one-dimensional, photon transport model was developed and tested for standard problems with known solutions published in the literature. The model simulated accurately the reflection and transmission of photons for all the cases considered.

The measured, canopy spectral reflectance of the burned and unburned grass canopies showed distinctly different diurnal trends in the visible and near to middle infrared regions of the spectrum. This was attributed to the presence of a layer of senescent vegetation in the unburned grass canopy and the sensor-sun-canopy azimuthal difference between the two canopies at the time of measurements. The observed

diurnal trends were more pronounced for off-nadir than nadir view angles, at all wavelengths for the two canopies. The model simulated properly the diurnal spectral characteristics of the burned and unburned canopies at an oblique (47.9^{o}) view angle for two different growing seasons.

The measured, seasonal trend in spectral characteristics showed consistently greater red reflectance for the unburned grass canopy than for the burned canopy, with comparable green leaf areas. The simulated, red reflectance values showed the same trend and compared well with the measured values. The measured, seasonal, infrared reflectance of the unburned treatment was smaller than that of the burned treatment, but the simulated reflectance values showed an opposite trend. This was attributed to a simplified representation of the role of senescent vegetation in the simulated results by the model. A more realistic representation of the role of this layer is required for proper simulation of spectral characteristics of the unburned grass canopy, especially in the infrared region.

Acknowledgement

We thank Dr. Blaine Blad and Mr. Patrick Stark for providing us some leaf optical property data. Mrs. Janet Killeen helped in preparing the figures, and Mrs. Pat Chapman typed the manuscript.

References

[1] Ransom, K.J., C.S.T. Daughtry, L.L. Biehl, and M.E. Bauer, "Sun-view angle effects on reflectance factors of corn canopies", Remote Sens. Environ., Vol. 18, pp. 147-161. 1985.

[2] Kimes, D. S., W. W. Newcomb, J. B. Schutt, P. J. Pinter, Jr., and R. D. Jackson, "Directional reflectance factor distributions of a cotton row crop". Int. J. Remote Sens., Vol. 5, pp. 263-277. 1984.

[3] Kollenkark, J.C., V.C. Vanderbilt, C.S.T. Daoughtry, and M.E. Bauer, "Influence of solar illumination angle on soybean canopy reflectance", Appl. Optics, Vol. 21, pp. 11279-1184, 1982.

[4] Ransom, K.J., L.L. Biehl and M.E. Bauer, "Variation in spectral response of soybeans with respect to illumination, view and canopy geometry", Int. J. Remote Sens., Vol. 6, pp. 1827-1842, 1985.

[5] Pinter, Jr., P.J., R.D. Jackson and H.W. Gausman, "Sun-angle and canopy-architecture effects on the spectral reflectance of six wheat cultivars", Int. J. Remote Sens., Vol. 6, pp. 1813-1825, 1985.

[6] Suits, G.H., "The calculation of directional reflectance of vegetative canopy", Remote Sens. Environ., Vol. 2, pp. 117-125, 1972.

[7] Suits, G.H., "Extension of a uniform canopy reflectance to include row effects", Remote Sens. Environ., Vol. 13, pp. 113-129, 1983.

[8] Bunnik, N.J.J., "The Multispectral Reflectance of shortwave radiation by agricultural crops in relation with their morphological and optical properties", Mededelingen Landbouwhogeschool, Wageningen, The Netherlands, 78-1, 1978.

[9] Norman, J.M. and J.M. Welles, "Radiative transfer in an array of canopies", Agron. J., Vol. 75, pp. 481-488, 1983.

[10] Kimes, D.S., "Modelling the directional reflectance from complete homogeneous vegetation canopies with various leaf-orientation distribution", Opt. Soc. Am. Ann., Vol. 1, pp. 725-738, 1984a.

[11] Myneni, R.B., J.P. Gutschick, J.K. Shultis, G. Asrar, and E.T. Kanemasu, "Photon transport in vegetation canopies with anisotropic scattering; Parts I through IV", Agric. Forest Meteorol., (submitted), 1987.

[12] Asrar, G., M. Yoshida and E.T. Kanemasu, "Estimates of leaf area index from spectral reflectance of wheat under different cultural practices and solar angle", Remote Sens. Environ., Vol. 17, pp. 1-11, 1985

[13] Bidwell, O.W., and McBee, C.W., "Soils of Kansas", Kansas Agric. Expt. Station, Dept. of Agron., Contribution No. 1359, 1973.

[14] The Tallgrass Laboratory, "Konza Prairie", Division of Biology, Kansas State Univ., Manhattan, KS 20 pp; 1984.

[15] Henderson, J.A., "Annual Precipitation Probabilities in Kansas", Bulletin No. 14, Kansas Water Resources Board, Topeka, Kansas, 107 pp., 1971.[17] Van de Hulst, H.C., "Multiple light scattering: Vols. I and II", Academic Press, New York, 1980.

[16] Kimball, B.A., "Smoothing data with cubic splines", Agron. J., Vol. 63, pp. 126-129, 1976.

[17] Van de Hulst, H.C., "Multiple light scattering: Vols. I and II", Academic Press, New York, 1980.

[18] Chandrasekhar, S., "Radiative transfer", Dover, New York, 1950.

[19] Asrar, G., R. L. Weiser, D. Johnson, E. T. Kanemasu and J. M. Killeen, "Distinguishing among tallgrass prairie cover types from measurements of multispectral reflectance", Remote Sens. Environ., Vol. 19, pp. 159-169, 1986.

[20] Ross, J., "The radiation regime and architecture of plant stands", Dr. W. Junk Publisher, The Netherlands, 1981.

List of Figures

Figure 11. Same as Figure 9, except for the near infrared region of the spectrum.

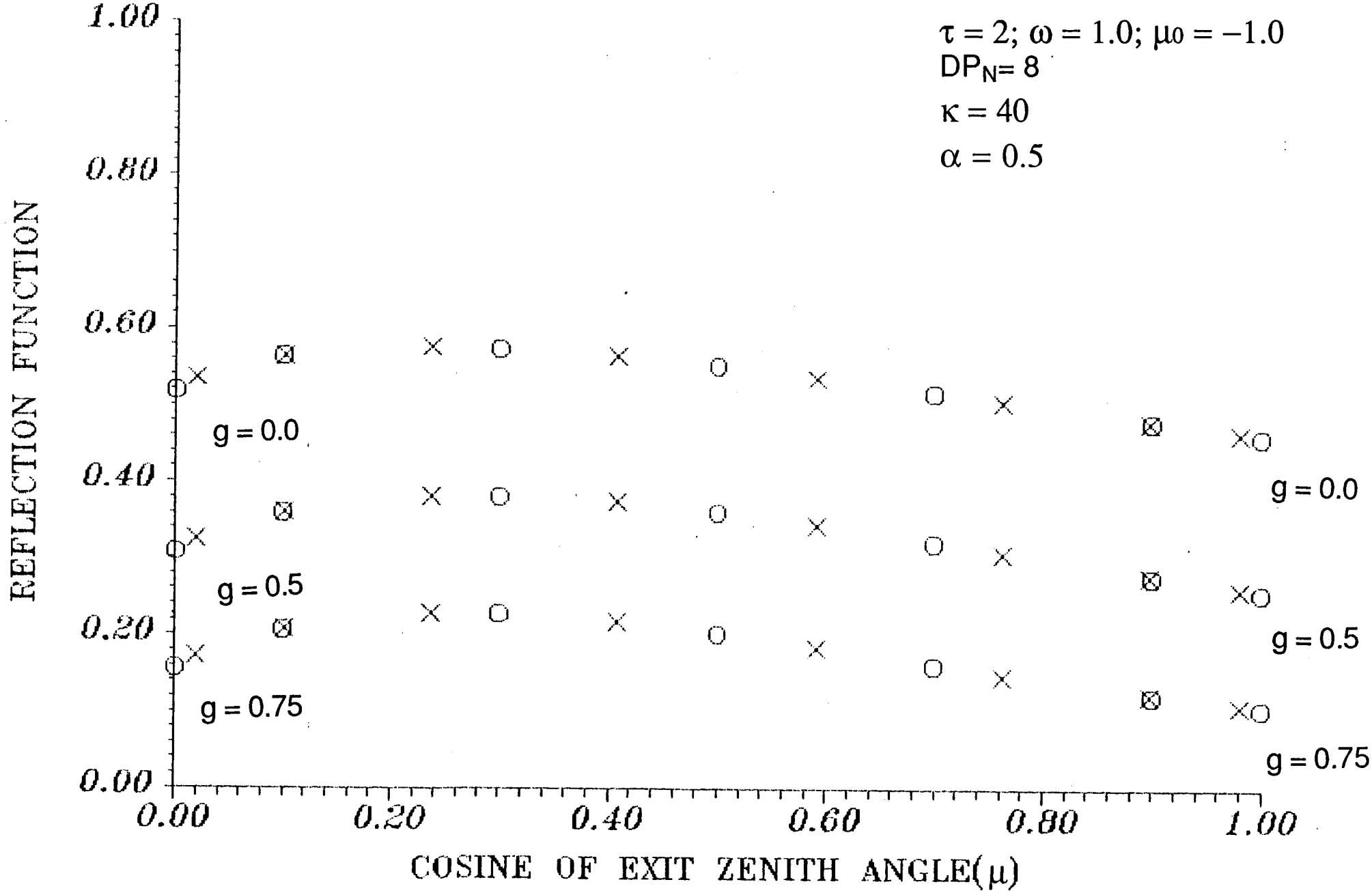
τ = 2; ω = 1.0; μ0 = −1.0
DP_N= 8
κ = 40
α = 0.5
1.00
0.80
0.60
0.40
0.20
0.00
REFLECTION FUNCTION
g = 0.0
g = 0.5
g = 0.75
g = 0.0
g = 0.5
g = 0.75
0.00
0.20
0.40
0.60
0.80
1.00
COSINE OF EXIT ZENITH ANGLE(μ)

Fig. 1

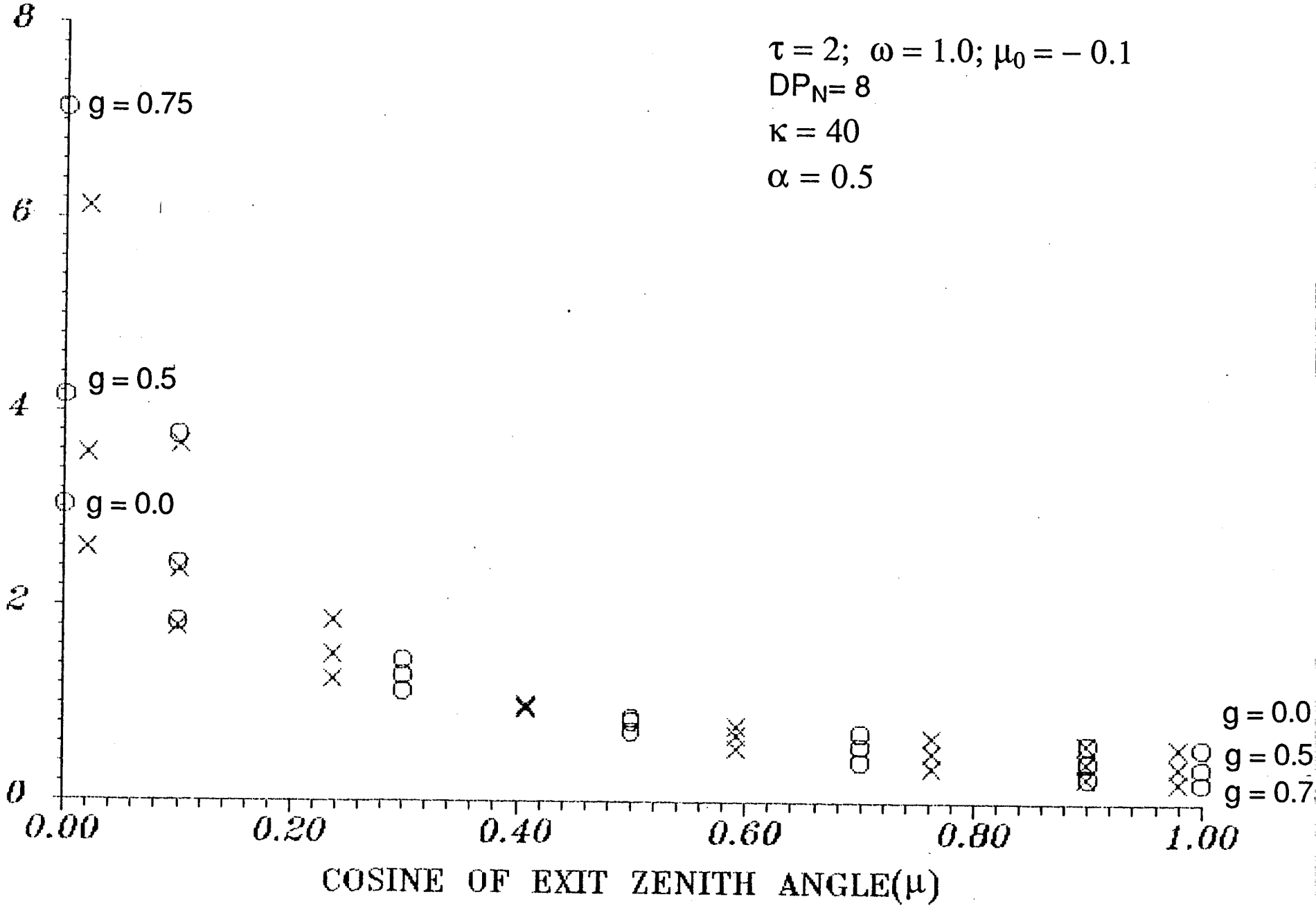
τ = 2; ω = 1.0; μ0 = – 0.1
DPN= 8
κ = 40
α = 0.5
g = 0.75
g = 0.5
g = 0.0
g = 0.0
g = 0.5
g = 0.7
REFLECTION FUNCTION
COSINE OF EXIT ZENITH ANGLE(μ)
0
2
4
6
8
0.00
0.20
0.40
0.60
0.80
1.00

Fig. 2

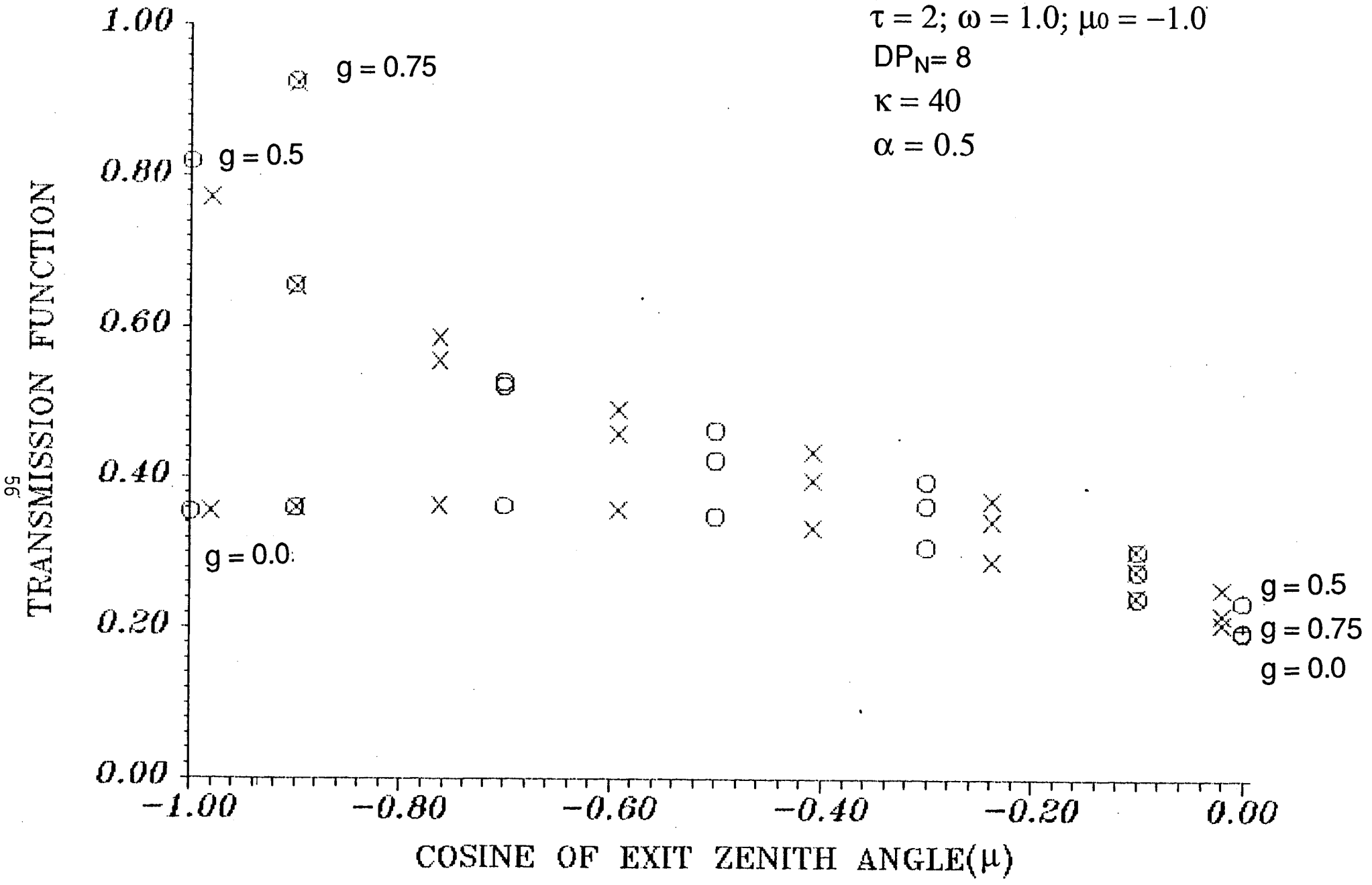
τ = 2; ω = 1.0; μ0 = −1.0
DP_N= 8
κ = 40
α = 0.5
g = 0.75
g = 0.5
g = 0.0
g = 0.5
g = 0.75
g = 0.0
TRANSMISSION FUNCTION
1.00
0.80
0.60
0.40
0.20
0.00
−1.00
−0.80
−0.60
−0.40
−0.20
0.00
COSINE OF EXIT ZENITH ANGLE(μ)

Fig. 3

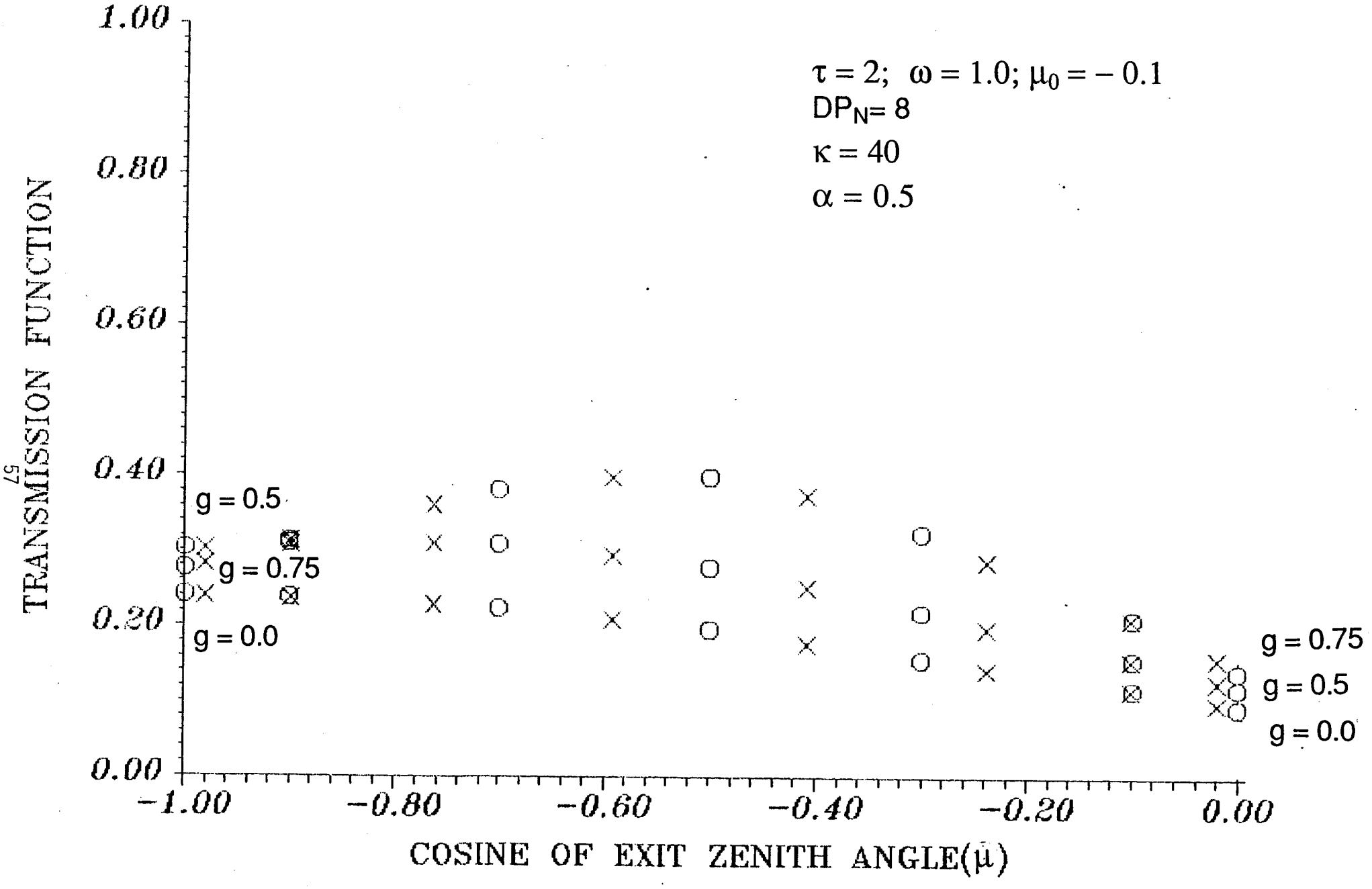
1.00
0.80
0.60
0.40
0.20
0.00
TRANSMISSION FUNCTION
τ = 2; ω = 1.0; μ0 = − 0.1
DPN= 8
κ = 40
α = 0.5
g = 0.5
g = 0.75
g = 0.0
g = 0.75
g = 0.5
g = 0.0
−1.00
−0.80
−0.60
−0.40
−0.20
0.00
COSINE OF EXIT ZENITH ANGLE(μ)

Fig. 4

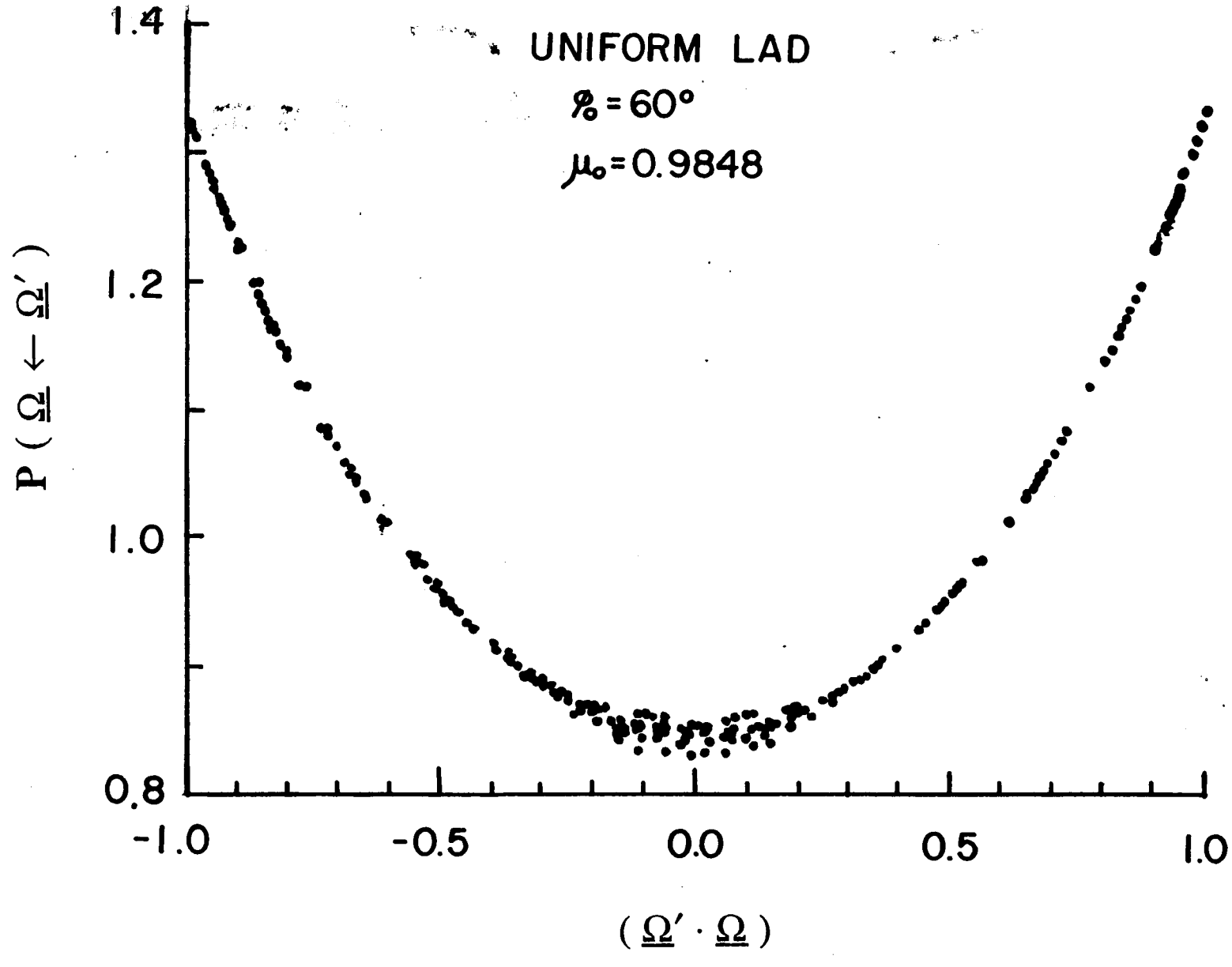
UNIFORM LAD
$\theta_0 = 60°$
$\mu_0 = 0.9848$
$P(\underline{\Omega} \rightarrow \underline{\Omega}')$
1.4
1.2
1.0
0.8
-1.0
-0.5
0.0
0.5
1.0
$(\underline{\Omega}' \cdot \underline{\Omega})$

Fig. 5

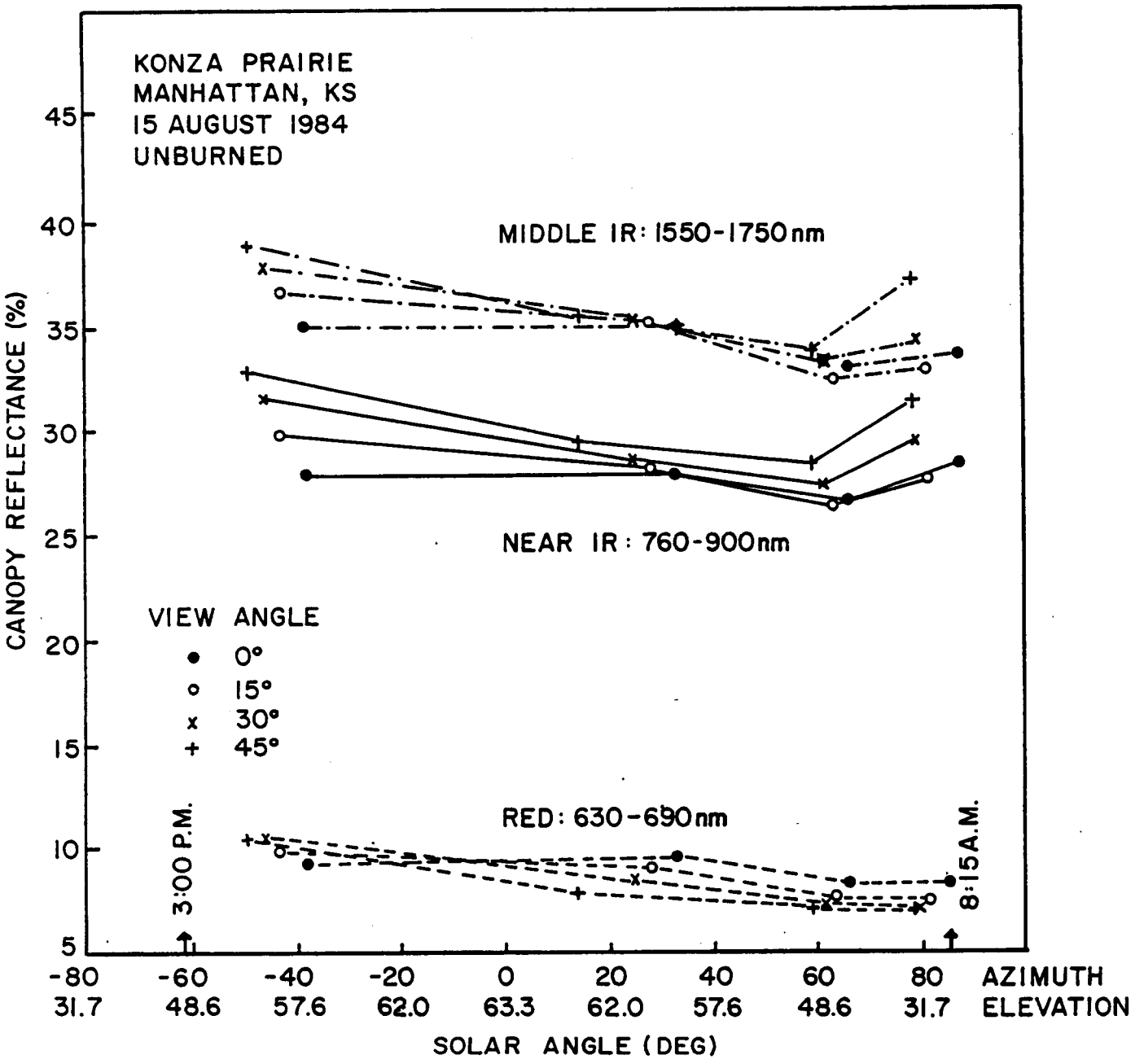
KONZA PRAIRIE
MANHATTAN, KS
15 AUGUST 1984
UNBURNED
MIDDLE IR: 1550-1750nm
NEAR IR: 760-900nm
RED: 630-690nm
VIEW ANGLE
0°
15°
30°
45°
3:00 P.M.
8:15 A.M.
CANOPY REFLECTANCE (%)
45
40
35
30
25
20
15
10
5
-80 -60 -40 -20 0 20 40 60 80 AZIMUTH
31.7 48.6 57.6 62.0 63.3 62.0 57.6 48.6 31.7 ELEVATION
SOLAR ANGLE (DEG)

Fig. 6

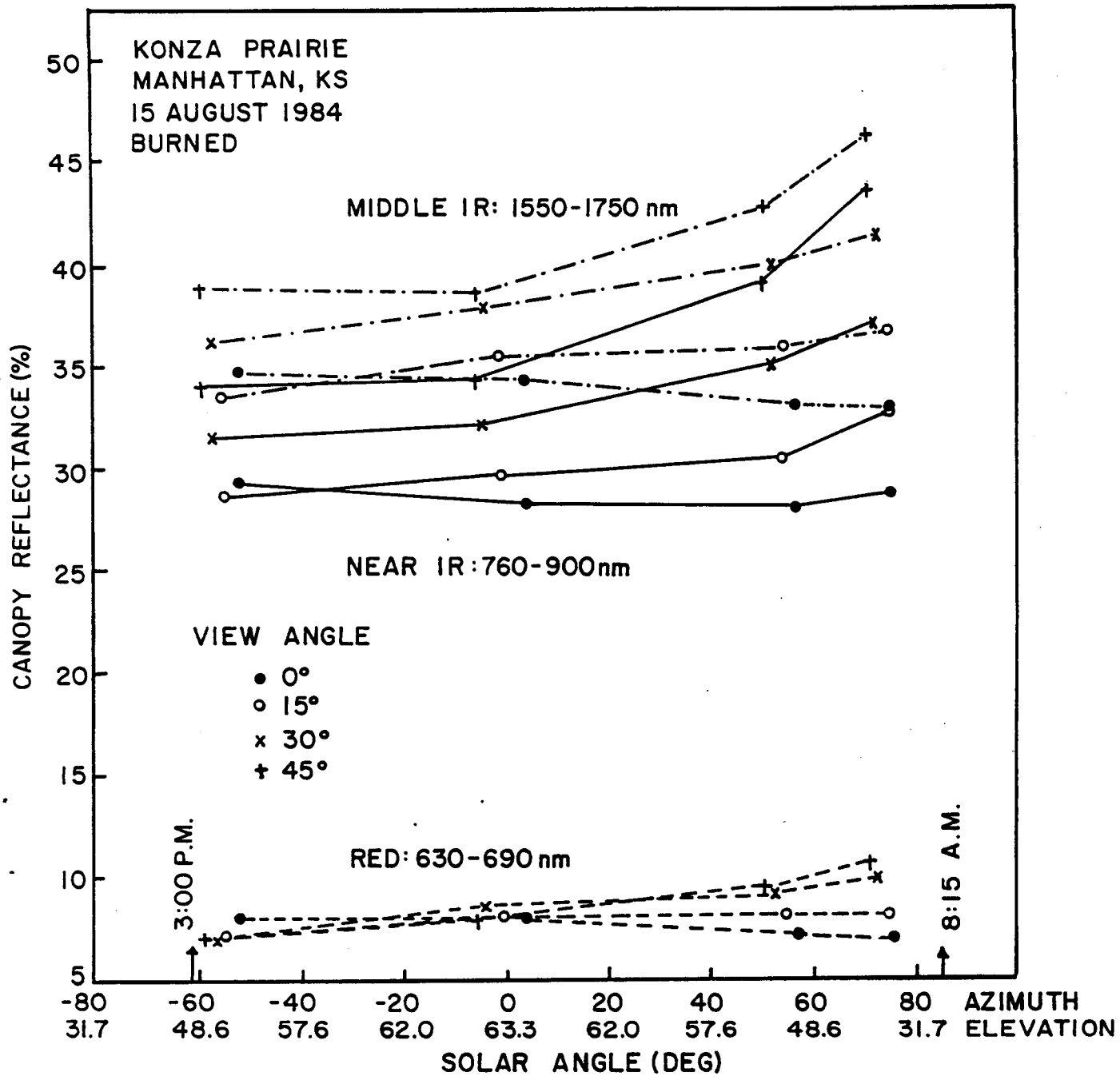
KONZA PRAIRIE
MANHATTAN, KS
15 AUGUST 1984
BURNED
MIDDLE IR: 1550-1750 nm
NEAR IR: 760-900nm
RED: 630-690 nm
VIEW ANGLE
• 0°
o 15°
x 30°
+ 45°
3:00 P.M.
8:15 A.M.
CANOPY REFLECTANCE (%)
50
45
40
35
30
25
20
15
10
5
-80 -60 -40 -20 0 20 40 60 80 AZIMUTH
31.7 48.6 57.6 62.0 63.3 62.0 57.6 48.6 31.7 ELEVATION
SOLAR ANGLE (DEG)

Fig. 7

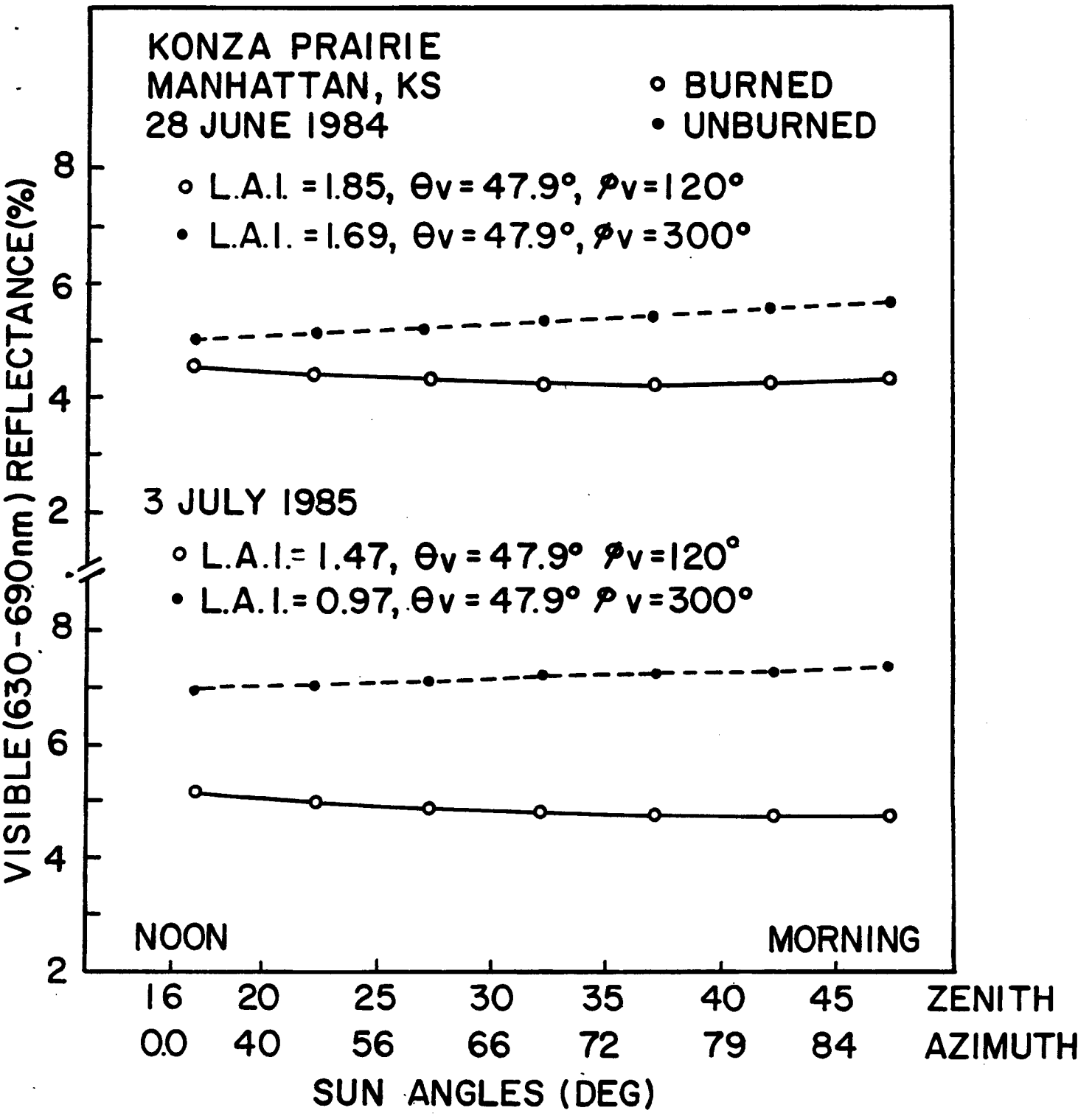
KONZA PRAIRIE
MANHATTAN, KS
28 JUNE 1984
o BURNED
• UNBURNED
o L.A.I. = 1.85, θv = 47.9°, ϕv = 120°
• L.A.I. = 1.69, θv = 47.9°, ϕv = 300°
3 JULY 1985
o L.A.I.= 1.47, θv = 47.9° ϕv = 120°
• L.A.I.= 0.97, θv = 47.9° ϕv = 300°
VISIBLE (630-690nm) REFLECTANCE (%)
NOON
MORNING
16 20 25 30 35 40 45 ZENITH
0.0 40 56 66 72 79 84 AZIMUTH
SUN ANGLES (DEG)

Fig. 8

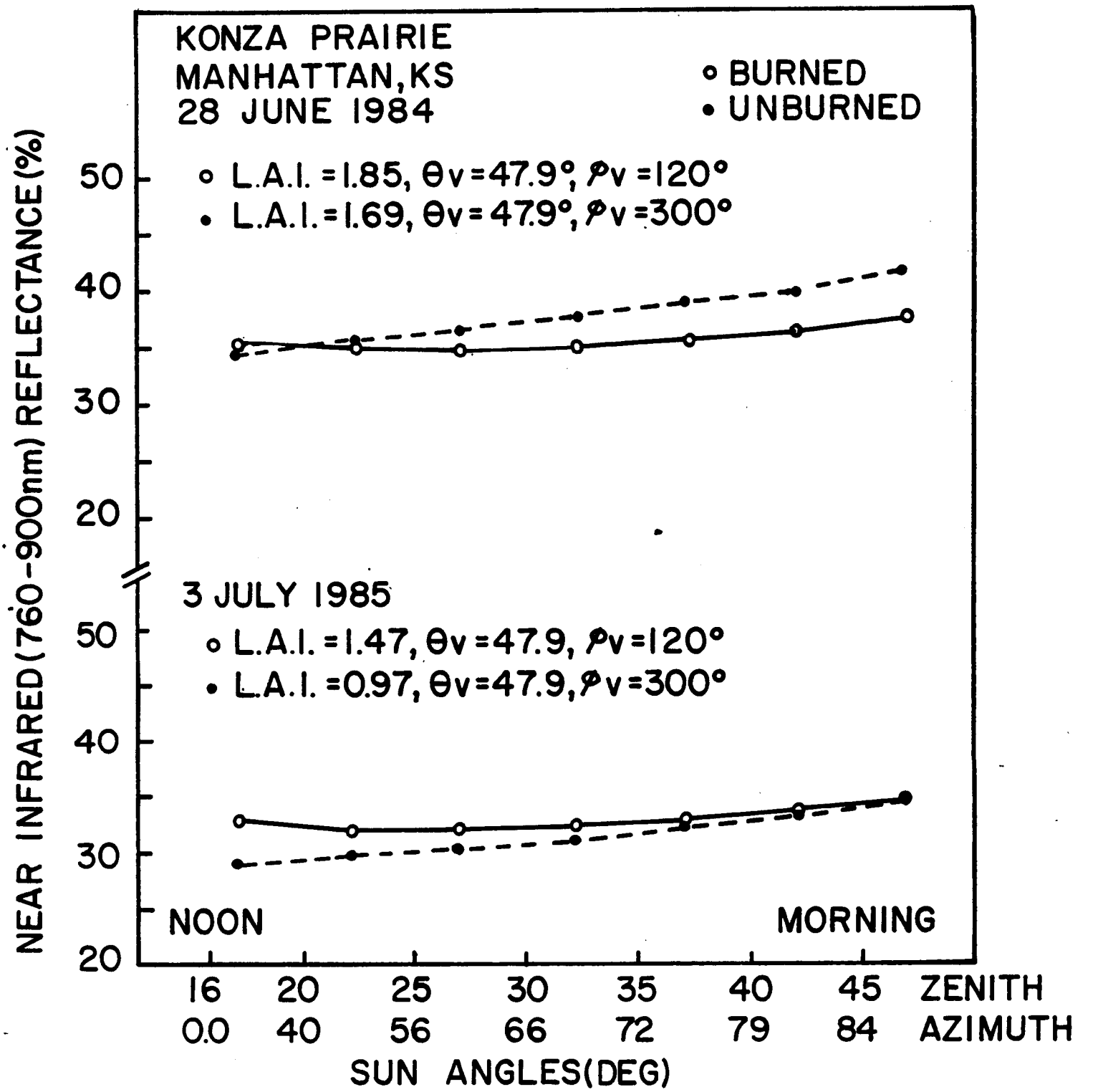
KONZA PRAIRIE
MANHATTAN, KS
28 JUNE 1984
o BURNED
• UNBURNED
o L.A.I. = 1.85, θv = 47.9°, φv = 120°
• L.A.I. = 1.69, θv = 47.9°, φv = 300°
3 JULY 1985
o L.A.I. = 1.47, θv = 47.9, φv = 120°
• L.A.I. = 0.97, θv = 47.9, φv = 300°
NEAR INFRARED (760-900nm) REFLECTANCE (%)
50
40
30
20
NOON
MORNING
16 20 25 30 35 40 45 ZENITH
0.0 40 56 66 72 79 84 AZIMUTH
SUN ANGLES (DEG)

Fig. 9

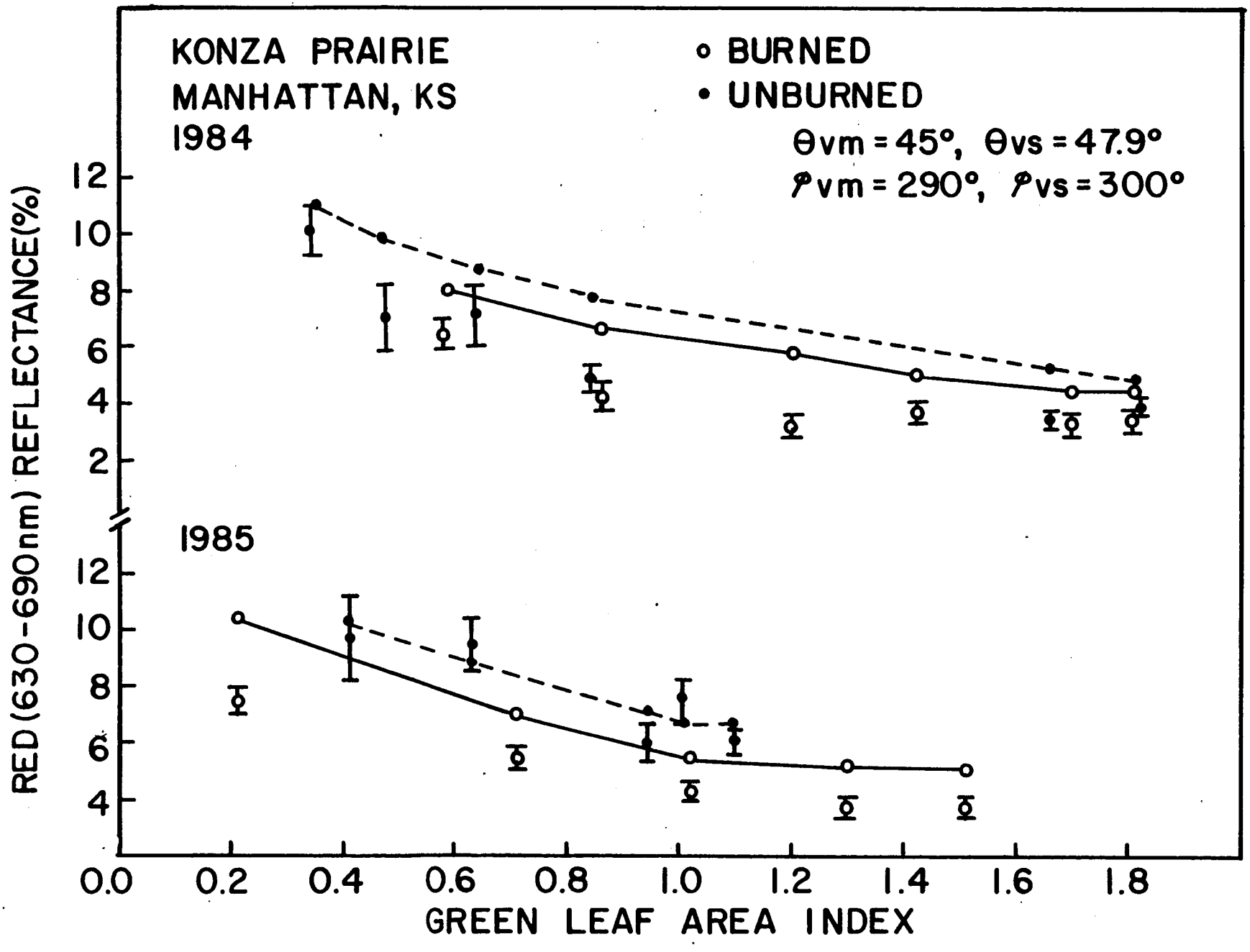
KONZA PRAIRIE
MANHATTAN, KS
1984
1985
o BURNED
• UNBURNED
Θvm = 45°, Θvs = 47.9°
φvm = 290°, φvs = 300°
RED (630-690nm) REFLECTANCE(%)
GREEN LEAF AREA INDEX
0.0
0.2
0.4
0.6
0.8
1.0
1.2
1.4
1.6
1.8
2
4
6
8
10
12

Fig. 10

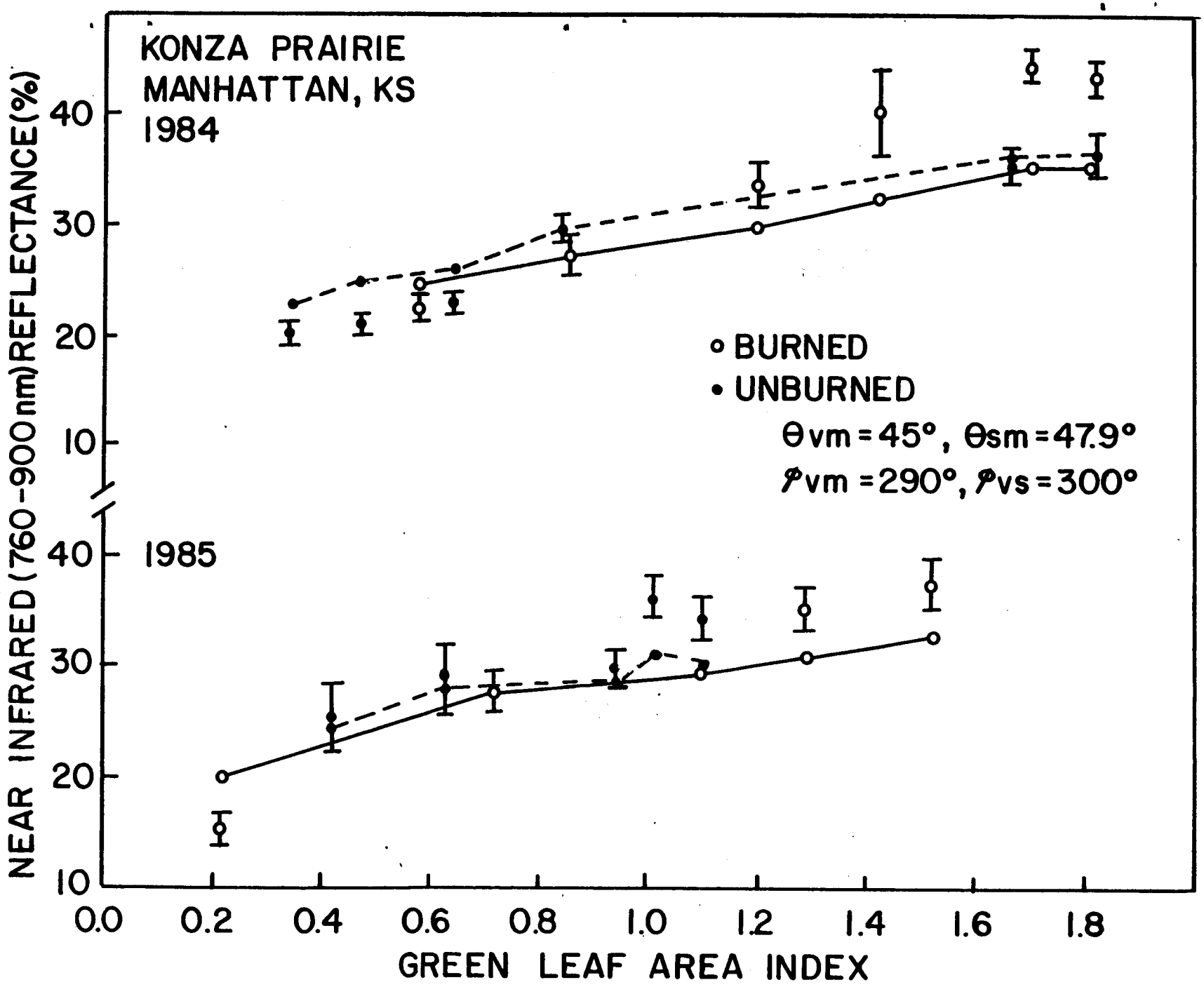
KONZA PRAIRIE
MANHATTAN, KS
1984
1985
BURNED
UNBURNED
θvm = 45°, θsm = 47.9°
φvm = 290°, φvs = 300°
NEAR INFRARED (760-900nm) REFLECTANCE (%)
GREEN LEAF AREA INDEX
10
20
30
40
0.0
0.2
0.4
0.6
0.8
1.0
1.2
1.4
1.6
1.8

Fig. 11